

Implementation of the force term in half-range lattice Boltzmann models

Victor E. Ambruş,^{1,2, a)} Victor Sofonea,^{1, b)} Richard Fournier,^{3, c)} and Stéphane Blanco^{3, d)}

¹⁾*Center for Fundamental and Advanced Technical Research,
Romanian Academy, Bd. Mihai Viteazul 24, 300223 Timișoara,
Romania*

²⁾*Department of Physics, West University of Timișoara, Bd. Vasile Pârvan 4,
300223 Timișoara, Romania*

³⁾*LAPLACE, Université de Toulouse, CNRS, INPT, UPS,
France.*

(Dated: 3 November 2021)

In the frame of the Boltzmann equation, wall-bounded flows of rarefied gases require the implementation of boundary conditions at the kinetic level. Such boundary conditions induce a discontinuity in the distribution function with respect to the component of the momentum which is normal to the boundary. Expanding the distribution function with respect to half-range polynomials allows this discontinuity to be captured. The implementation of this concept has been reported in the literature only for force-free flows. In the case of general forces which can have non-zero components in the direction perpendicular to the walls, the implementation of the force term requires taking the momentum space gradient of a discontinuous function. Our proposed method deals with this difficulty by employing the theory of distributions. We validate our procedure by considering the simple one-dimensional flow between diffuse-reflective walls of equal or different temperatures driven by the constant gravitational force. For this flow, a comparison between the results obtained with the full-range and the half-range Gauss-Hermite LB models is also presented.

^{a)}Corresponding author; victor.ambrus@e-uvt.ro

^{b)}sofonea@acad-tim.tm.edu.ro

^{c)}richard.fournier@laplace.univ-tlse.fr

^{d)}stephane.blanco@laplace.univ-tlse.fr

I. INTRODUCTION

Force-driven flows at microscale exhibit a plethora of applications^{1,2}, such as microelectrokinetics³⁻⁵, microscale cell manipulation⁵, deposition in particle laden turbulent flows⁶, as well as plasma flows⁷. While at the Navier-Stokes level, there are already established solvers for force-driven flows, the realm of microfluidics, where the Knudsen number Kn (defined as the ration between the mean free path of the constituents of the flow and the typical size of the flow domain) is non-negligible, is still not sufficiently well explored. Such systems can be accurately described at a mesoscopic level, using the one-particle distribution function $f \equiv f(\mathbf{x}, \mathbf{p}, t)$ for particles with momentum \mathbf{p} at position \mathbf{x} and time t , which evolves according to the Boltzmann equation.

At small values of Kn , the flow is close to equilibrium, such that the lattice Boltzmann (LB) models constructed using the full-range Gauss-Hermite quadratures yield accurate results⁸⁻¹⁰. As Kn is increased, the kinetic nature of the gas, as well as of the boundary conditions (which affect only the distribution of particles travelling from the wall back into the fluid), become important, giving rise to microfluidics-specific effects, such as velocity slip and temperature jump at the boundary¹¹⁻¹⁶. Such effects are due to the development of a discontinuity in the distribution function, which is best understood for the case of a collisionless gas: the particles travelling towards the wall are distributed according to some essentially arbitrary incident flux, while the distribution of reflected particles (which travel away from the wall and back into the fluid domain) is determined by the mechanism of interaction with the wall. In the case of diffuse reflection¹⁷, the particle-wall interaction causes the incident flux of particle to relax towards the equilibrium distribution of the wall before being reemitted back into the fluid domain. While other models are also possible, in general similar discontinuities in the distribution function will be induced between the incident and emergent hemispheres of the momentum space, essentially because the particles emerging from the boundary carry some information about the wall which is unavailable to incident particles prior to their interaction with the wall.

The correct treatment of diffuse reflection boundary conditions and the subsequent induced discontinuous nature of the distribution function requires the evaluation of half-space integrals, defined as integrals restricted to half of the momentum space^{11,18-23}.

Such half-space integrals can be accurately recovered using LB models based on half-

range quadratures^{24–41}. Using one quadrature per hemisphere, wall-induced hemispheric discontinuities are appropriately handled and we have shown, via a systematic set of simulation examples, that using half-range quadratures leads to accuracy gains in the rarefied regimes of the Couette^{38,40,42} and Poiseuille^{37,41} flows. This theoretical framework cannot be extended in a straightforward manner to force-driven flows where the force has a non-vanishing component in the direction perpendicular to the wall. Instead, the extension must be made with care, in order to avoid zeroth order errors (i.e. mass non-conservation) when the force is not strictly parallel to the boundary (we will address this point using a particular example starting from Eq. (1.1)). Such problems were not present in the simulations of Ref. 37 because the forces were parallel to the boundaries. In order to allow the half-range Gauss quadrature concept to be applied for flows in more complex force fields, we therefore reconsidered our theoretical framework with a specific attention to the component of the external forces which is perpendicular to the boundary.

The implementation of the force term in LB simulations requires a model to represent the momentum gradient $\nabla_p f$ of the distribution function f ⁹. For the case of LB models based on the full-range Hermite polynomials, f and $\partial_p f$ are both projected onto the space of full-range Hermite polynomials, as described in Ref. 43. Such a projection is possible since the full-range Hermite polynomials are continuous and differentiable everywhere in the momentum space. We wish to apply a similar procedure to the case when half-range quadratures are employed, with the aid of which physical configurations where f is not differentiable with respect to p at the interface between the two hemispheres (defined by the presence of the wall) can also be addressed.

To gain some insight on the difficulties associated with this discontinuity, it is instructive to consider the simple example of a one-dimensional uniform flow of a collisionless gas, subjected to a force F along the x axis. The Boltzmann equation in this case reads:

$$\partial_t f + F \partial_p f = 0. \tag{1.1}$$

Taking the full moment with respect to p of the above equation shows that the density remains constant through time:

$$\partial_t n = 0. \tag{1.2}$$

We now wish to implement Eq. (1.1) using half-range quadratures. Taking the half-range

moments of Eq. (1.1) over the positive and negative semiaxes yields:

$$\partial_t n_+ + F[f(\infty) - f(0_+)] = 0, \quad \partial_t n_- + F[f(0_-) - f(-\infty)] = 0, \quad (1.3)$$

where $f(0_+) \equiv \lim_{\substack{p \rightarrow 0 \\ p > 0}} f(p)$ and $f(0_-) \equiv \lim_{\substack{p \rightarrow 0 \\ p < 0}} f(p)$, while n_{\pm} are defined as:

$$n_+ = \int_0^{\infty} dp f, \quad n_- = \int_{-\infty}^0 dp f. \quad (1.4)$$

Assuming that $f(p)$ vanishes at $p \rightarrow \pm\infty$, the sum of the expressions in Eq. (1.3) yields:

$$\partial_t n = f(0_+) - f(0_-), \quad (1.5)$$

which reduces to Eq. (1.2) only when $f(p)$ is continuous at $p = 0$. It is important to note that $f(0_+) - f(0_-)$ is fully independent of the quadrature refinement used to evaluate Eq. (1.3). The difficulty identified here is not of numerical origin: it is a zeroth order bias that will never vanish by refining the numerical method (e.g. by increasing the spatial or temporal resolution, or by increasing the quadrature order). Thus, a strict application of the standard methodology presented in Ref. 43 to the case of half-range quadratures, when f is allowed to develop a discontinuity at $p = 0$, leads to spurious mass non-conservation as soon as the distribution function becomes discontinuous at $p = 0$.

In this paper, we present a procedure for the construction of the momentum gradient $\partial_p f$ of the distribution function f for force-driven flows when f is projected on the space of half-range polynomials. Fundamental to this construction is the theory of distributions, which allows f to be written using Heaviside step functions, the derivative of which are modelled as delta Dirac functions. The full details of this construction will be presented in section III. Based on this analysis, we give the recipe for the numerical implementation of $\partial_p f$ in LB models based on half-range Gauss quadratures, such as those introduced in Refs. 38 and 40.

In this paper, we restrict our analysis with no loss of generality to one-dimensional flows. The extension to 2- or 3-dimensional flows is straightforward through a direct-product procedure, as described in Refs.^{40,41}. The details regarding this extension are summarised in Appendix A.

The outline of this paper is as follows. In Sec. II, the expansion of $\partial_p f$ with respect to the full-range Hermite polynomials is discussed. The expansion of $\partial_p f$ with respect to general

half-range polynomials is presented in Sec. III. This is the main result of this paper. The construction of lattice Boltzmann models for force-driven flows using either full-range or the half-range Gauss quadratures is presented in Sec. IV. The numerical results are presented in Sec. V and Sec. VI concludes this paper.

Throughout this paper, we employ only non-dimensional quantities, following the convention of Refs. 18, 20–22, and 42.

II. EXPANSION OF $\partial_p f$ WITH RESPECT TO THE FULL-RANGE HERMITE POLYNOMIALS

The expansion of the momentum derivative of the distribution function with respect to the full-range Hermite polynomials has already been discussed in, e.g., Refs. 9 and 41. In this section, we briefly review the main results in order to prepare the terrain for the equivalent construction when half-range polynomials are considered. The starting point for our analysis is the one-dimensional Boltzmann-BGK equation in the presence of an external force F :

$$\partial_t f + \frac{p}{m} \partial_x f + F(\partial_p f) = -\frac{1}{\tau} (f - f^{(\text{eq})}), \quad (2.1)$$

where $f \equiv f(p, x, t)$ is the distribution function for particles of momentum p , $f^{(\text{eq})}$ is the Maxwell-Boltzmann equilibrium distribution function:

$$f^{(\text{eq})} = ng, \quad g \equiv g(u, T; p) = \frac{1}{\sqrt{2\pi mT}} \exp\left[-\frac{(p - mu)^2}{2mT}\right], \quad (2.2)$$

while τ is the relaxation time, which we implement as¹⁶:

$$\tau = \frac{\text{Kn}}{n}. \quad (2.3)$$

In this paper, we restrict our analysis without loss of generality to one-dimensional flows. The procedure presented herein is easily extendible to two- or three-dimensional flows, following the methodology presented in Appendix A.

We first start with the expansion of f with respect to the set $\{H_\ell(\bar{p}), \ell = 0, 1, \dots\}$ of full-range Hermite polynomials:

$$f = \frac{\omega(\bar{p})}{p_0} \sum_{\ell=0}^{\infty} \frac{1}{\ell!} \mathcal{F}_\ell H_\ell(\bar{p}), \quad (2.4)$$

where $\bar{p} = p/p_0$ is the ratio of the momentum p and some arbitrary momentum scale p_0 . We employ the following weight function:

$$\omega(\bar{p}) = \frac{1}{\sqrt{2\pi}} e^{-\bar{p}^2/2}, \quad (2.5)$$

while the normalisation condition for the Hermite polynomials reads:

$$\langle H_\ell, H_{\ell'} \rangle \equiv \int_{-\infty}^{\infty} dx H_\ell(x) H_{\ell'}(x) = \ell! \delta_{\ell, \ell'}. \quad (2.6)$$

The orthogonality relation (2.6) allows the expansion coefficients \mathcal{F}_ℓ to be obtained as:

$$\mathcal{F}_\ell = \int_{-\infty}^{\infty} dp f H_\ell(\bar{p}). \quad (2.7)$$

The expansion (2.4) is exact since the Hermite polynomials satisfy the following completeness relation:

$$\sum_{\ell=0}^{\infty} \frac{1}{\ell!} H_\ell(x) H_\ell(x') = \frac{\delta(x-x')}{\sqrt{\omega(x)\omega(x')}}. \quad (2.8)$$

The momentum derivative $\partial_p f$ can be obtained by differentiating Eq. (2.4) with respect to p :

$$\partial_p f = -\frac{\omega(\bar{p})}{p_0^2} \sum_{\ell=0}^{\infty} \frac{1}{\ell!} \mathcal{F}_\ell H_{\ell+1}(\bar{p}), \quad (2.9)$$

where the following relation was used^{41,44}:

$$\partial_x [\omega(x) H_\ell(x)] = -\omega(x) H_{\ell+1}(x). \quad (2.10)$$

Using the result (2.7), Eq. (2.9) can be written as:

$$[\partial_p f](p) = \int_{-\infty}^{\infty} dp' \mathcal{K}^H(p, p') f(p'), \quad (2.11)$$

where the kernel function $\mathcal{K}^H(p, p')$ is given by:

$$\mathcal{K}^H(p, p') = -\frac{\omega(\bar{p})}{p_0^2} \sum_{\ell=0}^{\infty} \frac{1}{\ell!} H_{\ell+1}(\bar{p}) H_\ell(\bar{p}'). \quad (2.12)$$

III. FORCE TERM IN LB MODELS BASED ON HALF-RANGE QUADRATURES

In this section, we derive an expression for the momentum gradient of the distribution function f in the case when f is expanded with respect to a family of half-range orthogonal

polynomials. For convenience, we restrict our derivation to the one-dimensional case, as done in the preceding section, and refer the interested reader to Appendix A for the extension to multiple dimensions. Before beginning, we would like to mention that the results derived in this section are very general and hold for any family of orthogonal polynomials defined on the Cartesian semiaxes and used in half-range LB models (e.g., the Laguerre polynomials³⁸ or the half-range Hermite polynomials^{40,41}).

A. Piece-wise decomposition of f

As suggested by Gross et al.⁴⁵, in wall-bounded flows, the distribution function $f(p)$ can be split with respect to the sign of p :

$$f(p) = \theta(p)f^+(p) + \theta(-p)f^-(p), \quad (3.1)$$

where $\theta(p)$ is the Heaviside step function, defined as:

$$\theta(p) = \begin{cases} 1 & p > 0, \\ 0 & \text{otherwise,} \end{cases} \quad \theta(p) + \theta(-p) = 1. \quad (3.2)$$

Such a piece-wise split is useful because it allows f to become discontinuous at $p = 0$, as is the case in, e.g., the ballistic regime of the Couette flow^{38,40,46}. Since the functions $f^+(p)$ and $f^-(p)$ are only defined for $p > 0$ and $p < 0$, respectively, the values $f^-(p = 0)$ and $f^+(p = 0)$ can be defined using the following limits:

$$f^-(0) = \lim_{\substack{p \rightarrow 0 \\ p < 0}} f^-(p), \quad f^+(0) = \lim_{\substack{p \rightarrow 0 \\ p > 0}} f^+(p). \quad (3.3)$$

In wall-bounded flows, $f^-(0)$ and $f^+(0)$ are in general not equal.

The two halves f^+ and f^- of the distribution function f can be expanded on $[0, \infty)$ and $(-\infty, 0]$, respectively, with respect to the set $\{\phi_\ell(|\bar{p}|), \ell = 0, 1, \dots\}$ of half-range orthogonal polynomials^{40,41} following the procedure used for the full-range case (2.4):

$$f^\sigma(p) = \frac{\omega(|\bar{p}|)}{p_0} \sum_{\ell=0}^{\infty} \frac{1}{\gamma_\ell} \mathcal{F}_\ell^\sigma \phi_\ell(|\bar{p}|), \quad (3.4)$$

where $\sigma = \pm$ refers to the sign of the argument p of f , as shown in Eq. (3.1), while γ_ℓ denotes the squared norm of $\phi_\ell \equiv \phi_\ell(z)$, $z \geq 0$:

$$\langle \phi_\ell, \phi_{\ell'} \rangle = \int_0^\infty dz \omega(z) \phi_\ell(z) \phi_{\ell'}(z) = \gamma_\ell \delta_{\ell, \ell'}. \quad (3.5)$$

The modulus in Eq. (3.4) ensures that the arguments of ω and ϕ_ℓ are always positive. The coefficients $\mathcal{F}_\ell^\sigma \equiv \mathcal{F}_\ell^\sigma(x, t)$ are independent of p and their exact expression can be obtained using the orthogonality relation (3.5):

$$\begin{aligned}\mathcal{F}_\ell^+ &= \int_0^\infty dp f(p) \phi_\ell(\bar{p}), \\ \mathcal{F}_\ell^- &= \int_{-\infty}^0 dp f(p) \phi_\ell(-\bar{p}) \\ &= \int_0^\infty dp f(-p) \phi_\ell(\bar{p}).\end{aligned}\tag{3.6}$$

The equality in Eq. (3.4) is exact if the polynomials $\phi_\ell(z)$ obey the completeness relation:

$$\sum_{\ell=0}^{\infty} \frac{1}{\gamma_\ell} \phi_\ell(z) \phi_\ell(z') = \frac{\delta(z - z')}{\sqrt{\omega(z)\omega(z')}},\tag{3.7}$$

B. Derivative of f with respect to the momentum

Applying the derivative operator with respect to p on Eq. (3.1) yields:

$$\frac{\partial f}{\partial p} = \theta(p) \frac{\partial f^+}{\partial p} + \theta(-p) \frac{\partial f^-}{\partial p} + \delta(p)[f^+(p) - f^-(p)],\tag{3.8}$$

where the Dirac delta function $\delta(p)$ is linked to the derivative of the step functions $\theta(\pm p)$ through⁴⁴:

$$\partial_p \theta(p) = \delta(p), \quad \partial_p \theta(-p) = -\delta(p).\tag{3.9}$$

It should be noted that the δ function is essential in order to preserve the standard requirement that the zeroth order moment of $\partial_p f$ vanishes:

$$\begin{aligned}\int_{-\infty}^{\infty} dp \frac{\partial f}{\partial p} &= \int_0^\infty dp \frac{\partial f^+}{\partial p} + \int_{-\infty}^0 dp \frac{\partial f^-}{\partial p} + [f^+(0) - f^-(0)] \\ &= 0.\end{aligned}\tag{3.10}$$

We now wish to project Eq. (3.8) on the semiaxes $[0, \infty)$ and $(-\infty, 0]$. Since $\theta(p) + \theta(-p) = 1$, the delta term can be included in both semiaxes:

$$\frac{\partial f}{\partial p} = \theta(p) \left(\frac{\partial f}{\partial p} \right)^+ + \theta(-p) \left(\frac{\partial f}{\partial p} \right)^-, \quad \left(\frac{\partial f}{\partial p} \right)^\sigma = \frac{\partial f^\sigma}{\partial p} + [\delta(p)]^\sigma [f^+(0) - f^-(0)],\tag{3.11}$$

where the factor multiplying the δ function is evaluated at $p = 0$ since at $p \neq 0$, the δ term vanishes. The distribution functions $f^\pm(0)$ are considered in the sense introduced in Eq. (3.3).

We next discuss the expansion of the δ term (Subsec. III C) and of $\partial_p f^\pm$ (Subsec. III D). The final result is summarised in Subsec. III E.

C. Expansion of the delta term

To find the expansion of $\delta(p)$ with respect to half-range polynomials, it is convenient to work with the following alternative definition of δ ⁴⁴:

$$\delta(p) = \lim_{\substack{\varepsilon \rightarrow 0 \\ \varepsilon > 0}} \delta_\varepsilon(p), \quad \delta_\varepsilon(p) = \frac{1}{\varepsilon\sqrt{\pi}} \exp\left(-\frac{p^2}{\varepsilon^2}\right). \quad (3.12)$$

Clearly, $\delta_\varepsilon(p)$ is a well-defined, even function everywhere, including at $p = 0$, as long as $\varepsilon > 0$. Its expansion with respect to half-range polynomials can be written as:

$$\delta_\varepsilon(p) = \theta(p) \frac{\omega(\bar{p})}{p_0} \sum_{\ell=0}^{\infty} \frac{1}{\gamma_\ell} \mathcal{F}_{\varepsilon,\ell}^{\delta,+} \phi_\ell(\bar{p}) + \theta(-p) \frac{\omega(-\bar{p})}{p_0} \sum_{\ell=0}^{\infty} \frac{1}{\gamma_\ell} \mathcal{F}_{\varepsilon,\ell}^{\delta,-} \phi_\ell(-\bar{p}). \quad (3.13)$$

Since $\delta_\varepsilon(-p) = \delta_\varepsilon(p)$, the expansion coefficients satisfy $\mathcal{F}_{\varepsilon,\ell}^{\delta,+} = \mathcal{F}_{\varepsilon,\ell}^{\delta,-} = \mathcal{F}_{\varepsilon,\ell}^{\delta}$. Their value can be calculated as in Eq. (3.6):

$$\begin{aligned} \mathcal{F}_{\varepsilon,\ell}^{\delta} &= \int_0^\infty dp \delta_\varepsilon(\pm p) \phi_\ell(\bar{p}) \\ &= \int_0^\infty \frac{dz}{\sqrt{\pi}} e^{-z^2} \phi_\ell\left(\frac{z\varepsilon}{p_0}\right). \end{aligned} \quad (3.14)$$

Taking the limit $\varepsilon \rightarrow 0$ in the above equation, the argument of ϕ_ℓ goes to 0, reducing $\mathcal{F}_{\varepsilon,\ell}^{\delta}$ to:

$$\lim_{\varepsilon \rightarrow 0} \mathcal{F}_{\varepsilon,\ell}^{\delta} = \frac{1}{2} \phi_{\ell,0}, \quad (3.15)$$

where the notation $\phi_{\ell,s}$ is introduced in Eq. (B1).

Thus, the expansion of $\delta(p)$ with respect to half-range polynomials is:

$$[\delta(p)]^\sigma = \frac{\omega(|\bar{p}|)}{2p_0} \Phi_0^\infty(|\bar{p}|), \quad (3.16)$$

where the notation $\Phi_s^\infty(z) = \lim_{n \rightarrow \infty} \Phi_s^n(z)$ is defined according to⁴⁰:

$$\Phi_s^n(z) = \sum_{\ell=s}^n \frac{1}{\gamma_\ell} \phi_{\ell,s} \phi_\ell(z). \quad (3.17)$$

The coefficient of $\delta(p)$ in Eq. (3.11) can also be projected with respect to the half-range polynomials by setting $p = 0$ in Eq. (3.4):

$$f^+(0) - f^-(0) = \frac{\omega(0)}{p_0} \sum_{\ell=0}^{\infty} \frac{1}{\gamma_\ell} (\mathcal{F}_\ell^+ - \mathcal{F}_\ell^-) \phi_{\ell,0}, \quad (3.18)$$

such that the projection of the full term $\delta(p)[f^+(0) - f^-(0)]$ appearing in Eq. (3.11) with respect to half-range polynomials becomes:

$$[\delta(p)]^\sigma [f^+(p) - f^-(p)] = \frac{\omega(|\bar{p}|)}{2p_0} \Phi_0^\infty(|\bar{p}|) \times \left[\frac{\omega(0)}{p_0} \sum_{\ell=0}^{\infty} (\mathcal{F}_\ell^+ - \mathcal{F}_\ell^-) \phi_{\ell,0} \right]. \quad (3.19)$$

D. The derivative of f^σ

Taking the derivative with respect to p of Eq. (3.4) gives:

$$\frac{\partial f^\sigma}{\partial p} = \frac{\sigma}{p_0^2} \sum_{\ell=0}^{\infty} \frac{1}{\gamma_\ell} \mathcal{F}_\ell^\sigma \left(\frac{\partial[\omega(z)\phi_\ell(z)]}{\partial z} \right)_{z=|\bar{p}|}. \quad (3.20)$$

Equation (B6) can be used to eliminate the above derivative with respect to z , giving:

$$\frac{\partial f^\sigma}{\partial p} = \frac{\sigma\omega(|\bar{p}|)}{p_0^2} \sum_{\ell=0}^{\infty} \mathcal{F}_\ell^\sigma \sum_{s=\ell+1}^{\infty} \frac{1}{\gamma_s} \varphi_{s,\ell} \phi_s(|\bar{p}|) - \frac{\sigma\omega(|\bar{p}|)}{p_0} \Phi_0^\infty(|\bar{p}|) \left[\frac{\omega(0)}{p_0} \sum_{\ell=0}^{\infty} \frac{1}{\gamma_\ell} \mathcal{F}_\ell^\sigma \phi_{\ell,0} \right], \quad (3.21)$$

where the term in the square bracket is equal to $f^\sigma(0)$, as can be seen by setting $p = 0$ in Eq. (3.4).

E. Final result

Adding Eqs. (3.16) and (3.21) gives:

$$\begin{aligned} \frac{\partial f}{\partial p} = \frac{\omega(|\bar{p}|)}{p_0^2} [\theta(p) - \theta(-p)] & \left[\sum_{\ell=0}^{\infty} \mathcal{F}_\ell^\sigma \sum_{s=\ell+1}^{\infty} \frac{1}{\gamma_s} \varphi_{s,\ell} \phi_s(|\bar{p}|) \right. \\ & \left. - \frac{\omega(0)}{2} \Phi_0^\infty(|\bar{p}|) \sum_{\ell=0}^{\infty} \frac{1}{\gamma_\ell} (\mathcal{F}_\ell^+ + \mathcal{F}_\ell^-) \phi_{\ell,0} \right]. \quad (3.22) \end{aligned}$$

The above result can be put into the form (2.11):

$$\frac{\partial f}{\partial p} = \int_{-\infty}^{\infty} dp' \mathcal{K}^{\text{half}}(p, p') f(p'), \quad (3.23)$$

where the kernel function $\mathcal{K}^{\text{half}}(p, p')$ is given by:

$$\begin{aligned} \mathcal{K}^{\text{half}}(p, p') = \frac{\omega(|\bar{p}|)}{p_0^2} [\theta(p) - \theta(-p)] \\ \times \left[\theta(pp') \sum_{\ell=0}^{\infty} \phi_\ell(|\bar{p}'|) \sum_{s=\ell+1}^{\infty} \frac{1}{\gamma_s} \phi_s(|\bar{p}|) \varphi_{s,\ell} - \frac{\omega(0)}{2} \Phi_0^\infty(|\bar{p}|) \Phi_0^\infty(|\bar{p}'|) \right]. \quad (3.24) \end{aligned}$$

Equation (3.24) represents the main result of this paper. It can be seen that the mixing between the regions with $p > 0$ and $p < 0$ occurs only due to the second term inside the square bracket. The implementation of Eq. (3.24) will be further discussed in Sec. IV B.

IV. LATTICE BOLTZMANN MODELS FOR FORCE-DRIVEN FLOWS

The basic ingredients for the construction of a lattice Boltzmann model to solve Eq. (2.1) are: 1) discretising the momentum space; 2) replacing the equilibrium distribution function $f^{(\text{eq})}$ in the collision term of Eq. (2.1) by a truncated polynomial; 3) replacing the momentum derivative of the distribution function in Eq. (2.1) using a suitable expression; 4) choosing a numerical method for the time evolution and spatial advection; and 5) implementation of the boundary conditions. A common feature of all lattice Boltzmann models is that the conservation equations for the particle number density n , macroscopic momentum density $n\mathbf{m}\mathbf{u}$ and temperature T (for thermal models) are exactly recovered.

Regardless of the chosen discretisation of the momentum space, the Boltzmann equation (2.1) becomes:

$$\partial_t f_k + \frac{p_k}{m} \partial_x f_k + F(\partial_p f)_k = -\frac{1}{\tau} (f_k - f_k^{(\text{eq})}), \quad (4.1)$$

where f_k ($k = 1, 2, \dots, \mathcal{Q}$) represents the set of distribution functions corresponding to the discrete momenta p_k . The total number \mathcal{Q} of discrete momenta depends on the particular quadrature. We will discuss in detail the implementation of steps 1) – 3) outlined above in LB models based on the full-range Gauss-Hermite quadratures (Subsec. IV A) and on general half-range quadratures, specialising the latter for the case of the Gauss-Laguerre and half-range Gauss-Hermite quadratures. (Subsec. IV B). In Subsec. IV C we present the numerical scheme employed in this paper for the time stepping and advection (step 4), as well as our implementation of the diffuse reflection boundary conditions (step 5). Finally, in Subsec. IV D we introduce the notation which can be used to distinguish between the 1D models employed in our simulations.

A. Full-range Gauss-Hermite quadrature

A full-range lattice Boltzmann model is constructed such that the full-range moments M_s of finite orders s of the distribution function f are exactly recovered:

$$M_s \equiv \int_{-\infty}^{\infty} dp f p^s = \sum_{k=1}^{\mathcal{Q}} f_k p_k^s. \quad (4.2)$$

1. Discretisation of the momentum space

Considering the expansion (2.4) with respect to the Gauss-Hermite polynomials, Eq. (4.2) becomes:

$$M_s = \sum_{\ell=0}^{\infty} \frac{1}{\ell!} \mathcal{F}_\ell \int_{-\infty}^{\infty} d\bar{p} \omega(\bar{p}) H_\ell(\bar{p}) p^s, \quad (4.3)$$

where the weight function $\omega(z)$ is defined in Eq. (2.5). The integral in Eq. (4.3) can be recovered using the Gauss-Hermite quadrature:

$$\int_{-\infty}^{\infty} dz \omega(z) P_s(z) \simeq \sum_{k=1}^Q w_k P_s(z_k), \quad (4.4)$$

where $P_s(z)$ is a polynomial of order s in z . The equality in Eq. (4.4) is exact if the number of quadrature points satisfies $2Q > s$. The quadrature points z_k are the roots of the Hermite polynomial $H_Q(z)$ of order Q , while their associated weights w_k are given by:

$$w_k = \frac{Q!}{[H_{Q+1}(\bar{p}_k)]^2}. \quad (4.5)$$

Thus, Eq. (4.2) is exact for $0 \leq s < Q$ if the expansion (2.4) is truncated at $\ell = Q$ and f_k is defined as:

$$f_k = \frac{w_k p_0}{\omega(p_k)} f^Q(p_k) = w_k \sum_{\ell=0}^{Q-1} \frac{1}{\ell!} \mathcal{F}_\ell H_\ell(\bar{p}_k). \quad (4.6)$$

It is worth mentioning that $\bar{p}_k = 0$, corresponding to stationary particles, is allowed in the set of discrete velocities only for odd quadrature orders Q . The implementation of diffuse reflection for such particles is problematic and the results obtained using models employing similar number of velocities are worse if the velocity set contains velocities which are parallel to the walls than in the case when such velocities are absent^{20,23,40,47-52}. We will therefore avoid the use of the HLB(N ; Q) models with odd Q in this work.

2. Hyperbolicity of the resulting scheme

As remarked in Ref. 6, choosing the discrete momenta to be linked to the roots of $H_Q(z)$ through $p_k = p_0 z_k$ automatically ensures that the truncation (4.6) of f_k with respect to the Hermite polynomials is preserved by the Boltzmann equation (4.1), provided f_k is initialised in the form in Eq. (4.6). This can be seen by casting the Boltzmann equation (2.1) in the following form:

$$\partial_t f + \frac{p}{m} \partial_x f = S, \quad (4.7)$$

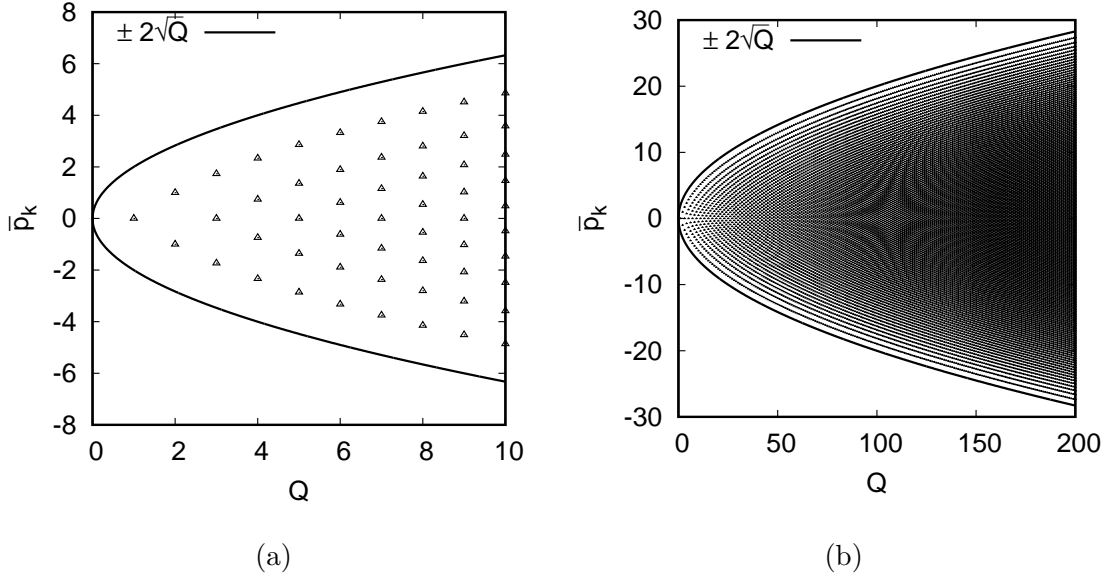


FIG. 1. Scatter plot of the quadrature points \bar{p}_k ($1 \leq k \leq Q$) occurring in the Gauss-Hermite quadrature of order Q for (a) $1 \leq Q \leq 10$ and (b) $1 \leq Q \leq 200$. At each value of Q represented on the horizontal axis, there are Q points on the corresponding vertical line, representing the values of the quadrature points \bar{p}_k . All quadrature points are contained inside the outer envelope $\pm 2\sqrt{Q}$.

where $S = -F\partial_p f - \frac{1}{\tau}(f - f^{(\text{eq})})$ is completely local (i.e., it does not involve spatial derivatives of f). Multiplying Eq. (4.7) by $H_\ell(\bar{p})$ and integrating with respect to the momentum space yields:

$$\partial_t \mathcal{F}_\ell + \partial_x A_{\ell,s} \mathcal{F}_s = \mathcal{S}_\ell, \quad (4.8)$$

where \mathcal{F}_ℓ is the coefficient corresponding to H_ℓ in the expansion (2.4) and \mathcal{S}_ℓ is defined in a similar manner:

$$S = \frac{\omega(\bar{p})}{p_0} \sum_{\ell=0}^{\infty} \frac{1}{\ell!} \mathcal{S}_\ell H_\ell(\bar{p}), \quad \mathcal{S}_\ell = \int_{-\infty}^{\infty} dp S H_\ell(\bar{p}). \quad (4.9)$$

The spatial derivative acts on a linear combination $A_{\ell,s} \mathcal{F}_s$ of \mathcal{F}_s , where the non-zero coefficients $A_{\ell,s}$ are:

$$A_{\ell,\ell+1} = \frac{p_0}{m}, \quad A_{\ell,\ell-1} = \frac{\ell p_0}{m}. \quad (4.10)$$

The above result is obtained by noting that $pH_\ell(\bar{p}) = p_0[H_{\ell+1}(\bar{p}) + \ell H_{\ell-1}(\bar{p})]$.

Employing a quadrature of order Q is equivalent to setting $\mathcal{F}_\ell = 0$ for all $\ell \geq Q$. This

allows $A_{\ell,s}$ to be represented as a $Q \times Q$ matrix of the form:

$$\mathbb{A} = \frac{p_0}{m} \begin{pmatrix} 0 & 1 & 0 & 0 & 0 & \cdots \\ 1 & 0 & 2 & 0 & 0 & \cdots \\ 0 & 1 & 0 & 3 & 0 & \cdots \\ 0 & 0 & 1 & 0 & 4 & \cdots \\ 0 & 0 & 0 & 1 & 0 & \cdots \\ \cdots & \cdots & \cdots & \cdots & \cdots & \cdots \end{pmatrix} \quad (4.11)$$

The system (4.8) is said to be hyperbolic if the matrix \mathbb{A} has only real eigenvalues $\lambda_s \in \mathbb{R}$ ($s = 1, 2, \dots, Q$). The system is strictly hyperbolic if the eigenvalues and their corresponding right eigenvectors \mathbb{K}_s are also distinct^{53,54}. At a fixed value of Q , the matrix \mathbb{A} (4.11) is truncated at $Q \times Q$ elements. In the following, we will consider the first few values of Q .

At $Q = 1$, $\mathbb{A} = (0)$ and $\lambda = 0$ with $\mathbb{K} = (1)$.

When $Q = 2$, we have:

$$\mathbb{A} = \frac{p_0}{m} \begin{pmatrix} 0 & 1 \\ 1 & 0 \end{pmatrix}, \quad \lambda_{\pm} = \pm \frac{p_0}{m}, \quad \mathbb{K}_{\pm} = \begin{pmatrix} 1 \\ \pm 1 \end{pmatrix}. \quad (4.12)$$

When $Q = 3$, the following values are obtained:

$$\mathbb{A} = \frac{p_0}{m} \begin{pmatrix} 0 & 1 & 0 \\ 1 & 0 & 2 \\ 0 & 1 & 0 \end{pmatrix}, \quad \lambda_0 = 0, \quad \lambda_{\pm} = \pm \frac{p_0 \sqrt{3}}{m}, \quad \mathbb{K}_0 = \begin{pmatrix} 1 \\ 0 \\ -1/2 \end{pmatrix}, \quad \mathbb{K}_{\pm} = \begin{pmatrix} 1 \\ \pm \sqrt{3} \\ 1 \end{pmatrix}. \quad (4.13)$$

It can be seen that, at fixed Q , the eigenvalues λ_s ($1 \leq \lambda_s \leq Q$) are linked to the roots \bar{p}_s of the Hermite polynomial $H_Q(\bar{p})$ of order Q through:

$$\lambda_s = \frac{p_0 \bar{p}_s}{m} = \frac{p_s}{m}. \quad (4.14)$$

This is also obvious since the projection of the Boltzmann equation (4.1) after discretisation onto the space of Hermite polynomials is equivalent to performing a linear transformation using the matrix:

$$\mathcal{H}_{\ell,k} = H_{\ell}(\bar{p}_k). \quad (4.15)$$

Applying the above transformation to the state vector f_k yields the state vector of the system of moment equations (4.8):

$$\sum_{k=1}^Q \mathcal{H}_{\ell,k} f_k = \mathcal{F}_{\ell}. \quad (4.16)$$

It is now clear that calculating the eigenvalues of the matrix $\mathcal{A}_{\ell,s}$ (4.10) is equivalent to calculating the eigenvalues of the matrix $\mathcal{A}_{k,k'}$, defined by writing Eq. (4.1) as:

$$\partial_t f_k + \partial_x (\mathcal{A}_{k,k'} f_{k'}) = S_k, \quad (4.17)$$

where it can be seen that $\mathcal{A}_{k,k'} = \frac{p_k}{m} \delta_{k,k'}$ is in diagonal form. Thus, the eigenvalues of \mathbb{A} (4.11) are nothing but the discrete velocities p_k/m corresponding to the Gauss-Hermite quadrature of order Q . These discrete velocities are necessarily distinct since they are linked to the roots of the Hermite polynomial of order Q . Thus, it can be seen that the system of lattice Boltzmann equations (4.1) is strictly hyperbolic for any choice of the quadrature order Q .

We end this section by illustrating the quadrature points corresponding to the Gauss-Hermite quadrature of various orders Q through a scatter plot in Fig. 1. It can be seen that for a fixed quadrature order $1 \leq Q \leq 200$, all quadrature points lie between $\pm 2\sqrt{Q}$. For completeness, we include in the supplementary material the roots and weights of the Gauss-Hermite quadrature up to $Q = 200$, as described in Appendix C.

3. Expansion of the equilibrium distribution function

Let us consider the expansion of g (2.2) in the form given in Eq. (2.4):

$$g = \frac{\omega(\bar{p})}{p_0} \sum_{\ell=0}^{\infty} \frac{1}{\ell!} \mathcal{G}_\ell H_\ell(\bar{p}). \quad (4.18)$$

Following the discretisation of the momentum space, $g(p)$ is replaced by g_k following the procedure in Eq. (4.6):

$$g_k = w_k \sum_{\ell=0}^N \frac{1}{\ell!} \mathcal{G}_\ell H_\ell(\bar{p}_k), \quad (4.19)$$

where the truncation order $N \leq Q - 1$ is a parameter of the model, representing the order up to which the moments of $f^{(\text{eq})}$ are exactly recovered using the Gauss-Hermite quadrature rule. The coefficients \mathcal{G} can be found using the orthogonality relation (2.6)^{40,41}:

$$\begin{aligned} \mathcal{G}_\ell &= \int_{-\infty}^{\infty} dp g H_\ell(\bar{p}) \\ &= \sum_{s=0}^{\lfloor \ell/2 \rfloor} \frac{\ell!}{2^s s! (\ell - 2s)!} \left(\frac{mT}{p_0^2} - 1 \right)^2 \left(\frac{mu}{p_0} \right)^{\ell - 2s}. \end{aligned} \quad (4.20)$$

4. Force term

We now turn to the implementation of the momentum derivative. This can be achieved by finding the equivalent $\mathcal{K}_{k,k'}$ after the discretisation of the momentum space of the kernel function $\mathcal{K}^H(p, p')$ (2.12). The definition of $\mathcal{K}_{k,k'}^H$ is the discrete analogue of Eq. (2.11):

$$(\partial_p f)_k = \sum_{k'=1}^Q \mathcal{K}_{k,k'}^H f_{k'}. \quad (4.21)$$

The sum over k' is obtained by converting the integral with respect to p' appearing in Eq. (2.11) into a quadrature sum following the prescription (4.4):

$$\int_{-\infty}^{\infty} dp' \mathcal{K}^H(p, p') f(p') \simeq \sum_{k'=1}^Q \mathcal{K}^H(p, p'_k) f_{k'}, \quad (4.22)$$

where the relation (4.6) between $f(p)$ and f_k was used. Since, by virtue of Eq. (4.6), $f_{k'}$ is a polynomial of order $Q - 1$ in p' , Eq. (4.22) is exact if $\mathcal{K}^H(p, p')$ is truncated at $\ell = Q - 1$. The terms corresponding to larger values of ℓ do not contribute to the integral (4.22) when f is a polynomial of order $Q - 1$, since the Hermite polynomials of orders $\ell > Q - 1$ are orthogonal to all polynomials of order $Q - 1$ or less by virtue of the orthogonality relation (2.6). Applying the relation (4.6) between $f(p)$ and f_k for the case of $\partial_p f$ and $(\partial_p f)_k$ allows $\mathcal{K}_{k,k'}^H$ to be written as:

$$\mathcal{K}_{k,k'}^H = -\frac{w_k}{p_0} \sum_{\ell=0}^{Q-2} \frac{1}{\ell!} H_{\ell+1}(\bar{p}_k) H_{\ell}(\bar{p}_{k'}), \quad (4.23)$$

where the sum over ℓ is truncated at $Q - 2$ since $H_{\ell+1}(p_k)$ vanishes when $\ell = Q - 1$. The resulting matrix $\mathcal{K}_{k,k'}^H$ has $Q \times Q$ elements, since $1 \leq k, k' \leq Q$. These elements can be computed at runtime, or they can be read from a data file. For the reader's convenience, we supply the matrix elements $\mathcal{K}_{k,k'}^H$ for $Q = 1, 2, \dots, 200$ in the supplementary material attached to this manuscript (more details are given in Appendix C).

B. Half-range quadratures

Half-range quadratures are employed to ensure the recovery of the half-range moments M_s^{\pm} of finite orders s of the distribution function f :

$$M_s^+ = \int_0^{\infty} dp f^+(p) p^s, \quad M_s^- = \int_{-\infty}^0 dp f^-(p) p^s. \quad (4.24)$$

1. Discretisation of the momentum space

The recovery of the half-range integrals in Eq. (4.24) can be achieved using half-range Gauss quadratures:

$$\int_0^\infty dz \omega(z) P_s(z) \simeq \sum_{k=1}^Q w_k P_s(z_k), \quad (4.25)$$

where the equality is exact if $2Q > s$. The quadrature points z_k ($k = 1, 2, \dots, Q$) are the Q (positive) roots of the half-range polynomial $\phi_Q(z)$, while the quadrature weights w_k are in general given by^{40,55,56}:

$$w_k = -\frac{a_Q \gamma_Q}{\phi_{Q+1}(|\bar{p}_k|) \phi'_Q(|\bar{p}_k|)}, \quad (4.26)$$

where $a_Q = \phi_{Q+1,Q+1}/\phi_{Q,Q}$ and $\phi_{\ell,s}$ represents the coefficient of z^s in $\phi_\ell(z)$, as described in Eq. (B1).

Considering the expansion (3.4) with respect to the half-range polynomials ϕ_ℓ , Eq. (4.24) becomes:

$$\begin{pmatrix} M_s^+ \\ M_s^- \end{pmatrix} = \sum_{\ell=0}^{\infty} \frac{1}{\ell!} \begin{pmatrix} \mathcal{F}_\ell^+ \\ \mathcal{F}_\ell^- \end{pmatrix} \int_0^\infty d\bar{p} \omega(\bar{p}) \phi_\ell(\bar{p}) (\pm p)^s. \quad (4.27)$$

Truncating the expansion (3.4) at $\ell = Q - 1$ ensures that a quadrature of order Q can recover the moments (4.27) for $0 \leq s \leq Q$. Since Q quadrature points are required on each semiaxis of the momentum space, the total number of elements in the momentum set is $\mathcal{Q} = 2Q$, defined as:

$$p_k = p_0 z_k, \quad p_{k+Q} = -p_k \quad (1 \leq k \leq Q). \quad (4.28)$$

Thus, the half-range moments (4.24) are recovered as:

$$M_s^+ = \sum_{k=1}^Q f_k p_k^s, \quad M_s^- = \sum_{k=Q+1}^{2Q} f_k p_k^s, \quad (4.29)$$

where

$$f_k = \frac{w_k p_0}{\omega(\bar{p}_k)} f(p_k), \quad f_{k+Q} = \frac{w_k p_0}{\omega(\bar{p}_k)} f(-p_k) \quad (1 \leq k \leq Q). \quad (4.30)$$

The quadrature weights w_k (4.26) are given in the case of the Gauss-Laguerre (w_k^L)^{37,38} and half-range Gauss-Hermite (w_k^h)^{40,41} quadratures through:

$$w_k^L = \frac{\bar{p}_k}{(Q+1)^2 [L_{Q+1}(\bar{p}_k)]^2}, \quad w_k^h = \frac{\bar{p}_k a_Q^2}{\mathfrak{h}_{Q+1}^2(\bar{p}_k) [\bar{p}_k + \mathfrak{h}_{Q,0}^2/\sqrt{2\pi}]}, \quad (4.31)$$

where a_ℓ is defined in Eq. (B11). The numerical values of the roots and quadrature weights for the half-range Gauss-Hermite quadratures with $1 \leq Q \leq 200$ can be found in the supplementary material, as described in Appendix C.

2. *Hyperbolicity of the resulting scheme*

We now perform the analysis presented in Sec. IV A 2 for the case of the LB models based on half-range quadratures. Multiplying Eq. (4.7) by $\phi_\ell(|\bar{p}|)$ and integrating with respect to \bar{p} over $[0, \infty)$ (+) and $(-\infty, 0]$ (-) yields:

$$\begin{aligned}\partial_t \mathcal{F}_\ell^+ + \partial_x A_{\ell,s}^+ \mathcal{F}_s^+ &= \mathcal{S}_\ell^+, \\ \partial_t \mathcal{F}_\ell^- + \partial_x A_{\ell,s}^- \mathcal{F}_s^- &= \mathcal{S}_\ell^-, \end{aligned} \quad (4.32)$$

where the matrices $A_{\ell,s}^\pm$ have the following non-zero elements:

$$A_{\ell,\ell-1}^\pm = \mp \frac{c_\ell p_0}{a_\ell m}, \quad A_{\ell,\ell}^\pm = \mp \frac{b_\ell p_0}{a_\ell m}, \quad A_{\ell,\ell+1}^\pm = \pm \frac{p_0}{a_\ell m}, \quad (4.33)$$

which are induced by the following recurrence relation:

$$\phi_{\ell+1}(z) = (a_\ell z + b_\ell) \phi_\ell(z) + \phi_{\ell-1}(z). \quad (4.34)$$

When the momentum space is discretized using a quadrature of order Q , the coefficients $\mathcal{F}_Q^\pm = 0$ and the matrices $A_{\ell,s}^\pm$ are of size $Q \times Q$. The functions \mathcal{F}_ℓ^+ and \mathcal{F}_ℓ^- corresponding to the projection of f on the positive and negative momentum semiaxes mix only due to the source function \mathcal{S}_ℓ , which can be expressed in completely local form with respect to \mathcal{F}_s^\pm . Thus, the hyperbolicity of the system of equations (4.32) can be analysed on each semiaxis independently. Moreover, Eq. (4.33) shows that $\mathbb{A}^+ = -\mathbb{A}^- = \mathbb{A}$, such that the eigenvalues of \mathbb{A}^- can be obtained from the eigenvalues of \mathbb{A}^+ by multiplying the latter by a factor of -1 . Hence, we will only focus on $\mathbb{A}^+ \equiv \mathbb{A}$, which can be written as follows:

$$\mathbb{A} = \frac{p_0}{m} \begin{pmatrix} -\frac{b_0}{a_0} & \frac{1}{a_0} & 0 & 0 & 0 & \dots \\ -\frac{c_1}{a_1} & -\frac{b_1}{a_1} & \frac{1}{a_1} & 0 & 0 & \dots \\ 0 & -\frac{c_2}{a_2} & -\frac{b_2}{a_2} & \frac{1}{a_2} & 0 & \dots \\ 0 & 0 & -\frac{c_3}{a_3} & -\frac{b_3}{a_3} & \frac{1}{a_3} & \dots \\ 0 & 0 & 0 & -\frac{c_4}{a_4} & -\frac{b_4}{a_4} & \dots \\ \dots & \dots & \dots & \dots & \dots & \dots \end{pmatrix} \quad (4.35)$$

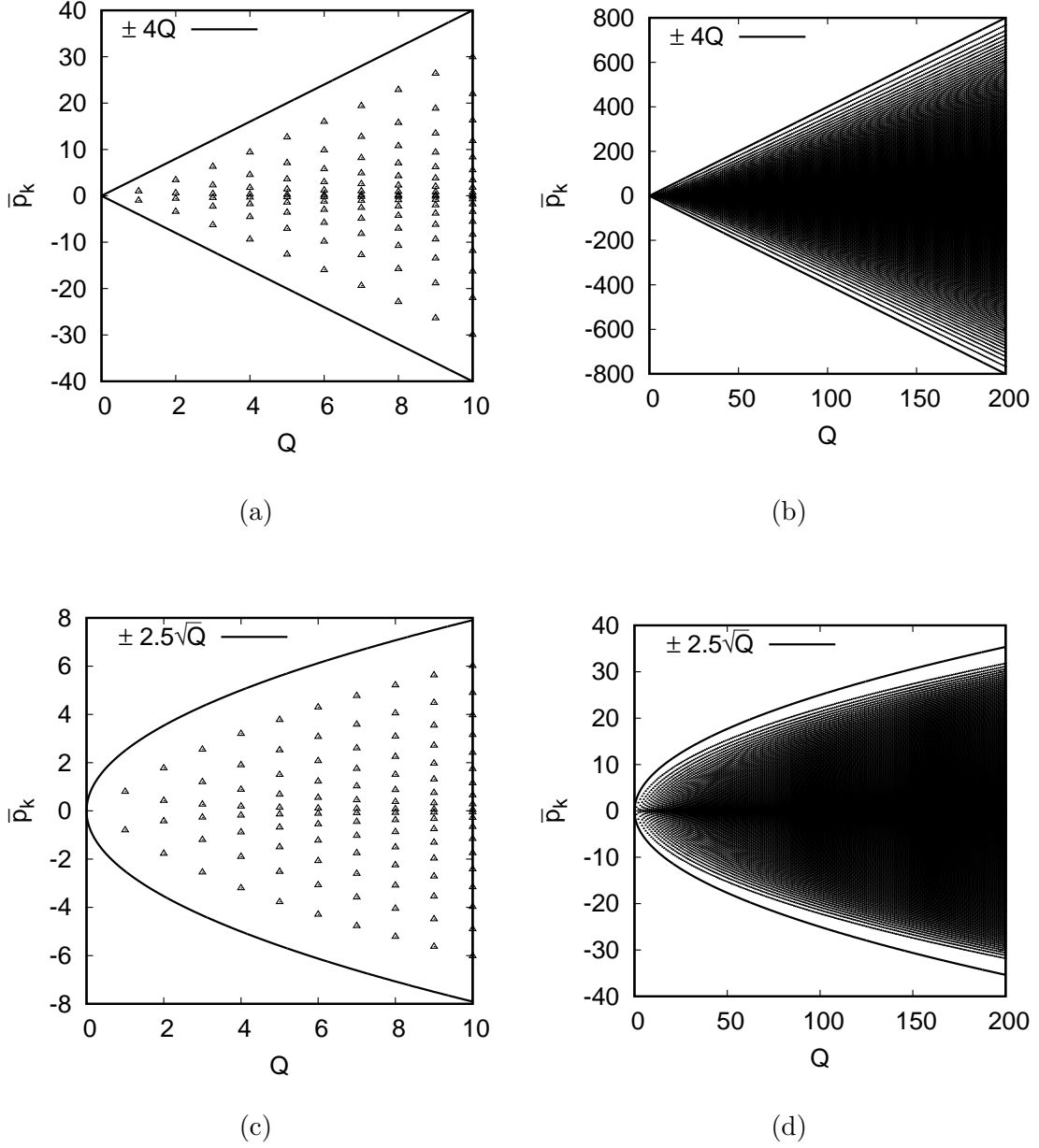


FIG. 2. Scatter plot of the quadrature points $\pm\bar{p}_k$ ($1 \leq k \leq Q$) occurring in the Gauss-Laguerre (top) and half-range Gauss-Hermite (bottom) quadratures of order Q , where $1 \leq Q \leq 10$ (left) and $1 \leq Q \leq 200$ (right). At each value of Q represented on the horizontal axis, there are $2Q$ points on the vertical line, representing the values of the quadrature points \bar{p}_k corresponding to the positive ($1 \leq k \leq Q$) and negative ($Q + 1 \leq k \leq 2Q$) semiaxes. All quadrature points are contained inside the outer envelope (a) $\pm 4Q$ for the Gauss-Laguerre quadrature and (b) $\pm 2.5\sqrt{Q}$ for the half-range Gauss-Hermite quadrature.

At $Q = 1$, the eigenvalue equation yields $\lambda = -\frac{p_0 b_0}{m a_0}$, which represents the root of $\phi_1(\bar{p})$ multiplied by p_0/m . Next, at $Q = 2$, the eigenvalue equation reads

$$a_0 a_1 \lambda^2 + (a_0 b_1 + a_1 b_0) \lambda + b_0 b_1 + c_1 = \frac{\phi_2(\lambda)}{\phi_0(\lambda)} = 0, \quad (4.36)$$

where the intermediate equality follows by applying the the recurrence relation (4.34) twice to obtain $\phi_2(\lambda)$ in terms of $\phi_0(\lambda)$. Eq. (4.36) shows that the eigenvalues of \mathbb{A}^+ when $Q = 2$ are the roots of $\phi_2(\lambda)$.

Thus we reach the same conclusion as for the case of the full-range Gauss-Hermite quadrature, which we summarise as follows. The system of moment equations (4.32) is obtained by applying a linear transformation on the lattice Boltzmann equation (4.1) using the matrices

$$\mathcal{H}_{\ell,k}^+ = \begin{cases} \phi_\ell(\bar{p}_k), & 1 \leq k \leq Q, \\ 0, & \text{otherwise} \end{cases} \quad \mathcal{H}_{\ell,k}^- = \begin{cases} \phi_\ell(-\bar{p}_k), & Q < k \leq 2Q, \\ 0, & \text{otherwise.} \end{cases} \quad (4.37)$$

Putting the Boltzmann equation in the form (4.17) shows that calculating the eigenvalues of the matrices $\mathcal{A}_{\ell,s}^+$ and $\mathcal{A}_{\ell,s}^-$ is equivalent to obtaining the eigenvalues of $\mathcal{A}_{k,k'} = \frac{p_k}{m} \delta_{k,k'}$, which are just the discrete velocities corresponding to the half-range Gauss quadrature of order Q , together with their reflection with respect to the origin. Since $p_k = p_0 \bar{p}_k$ ($1 \leq k \leq Q$) is linked to the roots of $\phi_Q(\bar{p})$, it is clear that the resulting eigenvalues are real and distinct and thus, the system of lattice Boltzmann equations (4.1) is strictly hyperbolic.

We end this section by showing a scatter plot of the quadrature points \bar{p}_k ($1 \leq k \leq 2Q$) for the Gauss-Laguerre [Fig. 2(a,b)] and half-range Gauss-Hermite [Fig. 2(c,d)] quadratures. The solid lines indicate that, at fixed Q , the quadrature points satisfy $-4Q < \bar{p}_k < 4Q$ and $-2.5\sqrt{Q} < \bar{p}_k < 2.5\sqrt{Q}$ in the case of the Gauss-Laguerre and half-range Gauss-Hermite quadratures, respectively.

3. Expansion of the equilibrium distribution function

In the case of half-range quadratures, the function g defined in Eq. (2.2) must be expanded separately on the positive and negative momentum semiaxes:

$$g_\sigma = \frac{\omega(|\bar{p}|)}{p_0} \sum_{\ell=0}^{\infty} \mathcal{G}_\ell^\sigma \phi_\ell(|\bar{p}|), \quad (4.38)$$

where $\sigma = 1$ when $p > 0$ and $\sigma = -1$ when $p < 0$. Following the convention of Eq. (4.28), the momentum space is discretised using $\mathcal{Q} = 2Q$ elements with $p_k > 0$ and $p_{k+Q} = -p_k$ for $1 \leq k \leq Q$. The corresponding equilibrium distributions $f_k^{(\text{eq})} = ng_k$ are constructed using

$$g_k = w_k \sum_{\ell=0}^N \mathcal{G}_\ell^+ \phi_\ell(\bar{p}_k), \quad g_{k+Q} = w_k \sum_{\ell=0}^N \mathcal{G}_\ell^- \phi_\ell(\bar{p}_k), \quad (4.39)$$

where the expansion order $0 \leq N < Q$ is a free parameter of the model which represents the order up to which the half-range moments of $f^{(\text{eq})}$ are exactly recovered. The coefficients \mathcal{G}_ℓ^\pm can be found using the orthogonality relation (3.5):

$$\mathcal{G}_\ell^+ = \int_0^\infty dp g \phi_\ell(\bar{p}), \quad \mathcal{G}_\ell^- = \int_{-\infty}^0 dp g \phi_\ell(-\bar{p}). \quad (4.40)$$

Irrespective of the choice of quadrature, \mathcal{G}_ℓ^\pm can be expressed analytically and g_k becomes^{40,41}:

$$g_k = \frac{w_k}{2} \sum_{s=0}^N \left(\frac{mT}{2p_0^2} \right)^{s/2} \Phi_s^N(\bar{p}_k) \left[(1 + \text{erf } \zeta) P_s^+(\zeta) + \frac{2}{\sqrt{\pi}} e^{-\zeta^2} P_s^*(\zeta) \right],$$

$$g_{k+Q} = \frac{w_k}{2} \sum_{s=0}^N \left(\frac{mT}{2p_0^2} \right)^{s/2} \Phi_s^N(\bar{p}_k) \left[(1 - \text{erf } \zeta) P_s^+(-\zeta) + \frac{2}{\sqrt{\pi}} e^{-\zeta^2} P_s^*(-\zeta) \right], \quad (4.41)$$

where $\zeta = u\sqrt{m/2T}$, $\Phi_s^N(\bar{p}_k)$ is defined in Eq. (3.17), while $P_s^+(\zeta)$ and $P_s^*(\zeta)$ represent polynomials of orders s and $s - 1$, respectively, defined through:

$$P_s^\pm(\zeta) = e^{\mp\zeta^2} \frac{d^s}{d\zeta^s} e^{\pm\zeta^2}, \quad P_s^*(\zeta) = \sum_{j=0}^{s-1} \binom{s}{j} P_j^+(\zeta) P_{s-j-1}^-(\zeta). \quad (4.42)$$

4. Force term

We have seen in Sec. III E that the kernel $\mathcal{K}^{\text{half}}(p, p')$ for the momentum derivative $\partial_p f$ mixes the distributions of particles on the two semiaxes. The full-range integral with respect to p' in Eq. (3.23) can be written as a sum of two half-range integrals over the domains $[0, \infty)$ and $(-\infty, 0]$, which can be recovered as follows:

$$(\partial_p f)_k = \sum_{k'=1}^{2Q} \mathcal{K}_{k,k'}^{\text{half}} f_{k'}. \quad (4.43)$$

In the above, $f_{k'}$ is a polynomial of order $Q - 1$ in $p_{k'}$. The equality in Eq. (4.43) can be achieved only if $\mathcal{K}^{\text{half}}(p, p')$ is truncated at order $Q - 1$ with respect to $\phi_\ell(p')$. This truncation still allows the exact recovery of the integral with respect to p' in Eq. (3.23) since

the polynomials $\phi_\ell(|\bar{p}'|)$ with $\ell \geq Q$ are orthogonal to all polynomials of order $Q - 1$ or less by virtue of the orthogonality relation (3.5).

We furthermore require the truncation of $\mathcal{K}^{\text{half}}(p, p')$ at $\ell = Q - 1$ with respect to $\phi_\ell(|\bar{p}|)$. This truncation allows the closure of the moment equation (4.32) with respect to \mathcal{F}_ℓ^\pm with $0 \leq \ell \leq Q - 1$. We note that the moments of order $0 \leq s < Q$ of $\partial_p f$ are exactly recovered when using the above truncation of $\mathcal{K}^{\text{half}}(p, p')$, since the polynomials $\phi_\ell(|\bar{p}|)$ with $\ell \geq Q$ do not contribute to the moments of order $0 \leq s < Q$ by virtue of the orthogonality relation (3.5).

The resulting expression for the kernel $\mathcal{K}_{k,k'}^{\text{half}}$ is:

$$\mathcal{K}_{k,k'}^{\text{half}} = \frac{w_k \sigma_k}{p_0} \left[\frac{1 + \sigma_k \sigma_{k'}}{2} \sum_{\ell=0}^{Q-2} \phi_\ell(|\bar{p}_{k'}|) \sum_{s=\ell+1}^{Q-1} \frac{1}{\gamma_s} \phi_s(|\bar{p}_k|) \varphi_{s,\ell} - \frac{\omega(0)}{2} \Phi_0^Q(|\bar{p}_k|) \Phi_0^Q(|\bar{p}_{k'}|) \right], \quad (4.44)$$

where $\sigma_k = 1$ when $1 \leq k \leq Q$ and $\sigma_k = -1$ when $Q < k \leq 2Q$. Let us now specialise Eq. (4.44) to the case of the Gauss-Laguerre and half-range Gauss-Hermite quadratures.

When the Gauss-Laguerre quadrature is employed, $\omega(z)$, γ_ℓ and $\varphi_{\ell,s}$ take the following values:

$$\omega(z) = e^{-z}, \quad \gamma_\ell = 1, \quad \varphi_{s,\ell} = \begin{cases} 1 & 0 \leq \ell < s, \\ 0 & \text{otherwise.} \end{cases} \quad (4.45)$$

In this case, Eq. (4.44) becomes:

$$\mathcal{K}_{k,k'}^L = \frac{w_k \sigma_k}{p_0} \left[\frac{1 + \sigma_k \sigma_{k'}}{2} \sum_{\ell=0}^{Q-2} L_\ell(|\bar{p}_{k'}|) \sum_{s=\ell+1}^{Q-1} L_s(|\bar{p}_k|) - \frac{1}{2} \Phi_0^Q(|\bar{p}_k|) \Phi_0^Q(|\bar{p}_{k'}|) \right], \quad (4.46)$$

where $\Phi_0^Q(|\bar{p}_k|)$, defined in Eq. (3.17), reduces to:

$$\Phi_0^Q(|\bar{p}_k|) = \sum_{s=0}^{Q-1} L_s(|\bar{p}_k|), \quad (4.47)$$

where the upper limit of the sum over s is $Q - 1$ since $L_Q(|\bar{p}_k|) = 0$.

In the case of the half-range Hermite polynomials, $\gamma_\ell = 1$ and $\varphi_{\ell,s}$ can be found in Eq. (B10). Thus, Eq. (4.44) becomes:

$$\mathcal{K}_{k,k'}^h = \frac{w_k \sigma_k}{p_0} \left\{ \frac{1 + \sigma_k \sigma_{k'}}{2} \sum_{\ell=0}^{Q-2} \mathfrak{h}_\ell(|\bar{p}_{k'}|) \left[\frac{\mathfrak{h}_{\ell,0}}{\sqrt{2\pi}} \sum_{s=\ell+1}^{Q-1} \mathfrak{h}_{s,0} \mathfrak{h}_s(|\bar{p}_k|) - \frac{\mathfrak{h}_{\ell,\ell}}{\mathfrak{h}_{\ell+1,\ell+1}} \mathfrak{h}_{\ell+1}(|\bar{p}_k|) \right] - \frac{1}{2\sqrt{2\pi}} \Phi_0^Q(|\bar{p}_k|) \Phi_0^Q(|\bar{p}_{k'}|) \right\}. \quad (4.48)$$

0		
1	1	
1/2	1/4	1/4
	1/6	2/3

TABLE I. Butcher tableau for the third-order Runge-Kutta time-stepping procedure described in Eq. (4.52).

where $\Phi_0^Q(|\bar{p}_k|)$ (3.17) reduces to:

$$\Phi_0^Q(|\bar{p}_k|) = \sum_{s=0}^{Q-1} \mathfrak{h}_{s,0} \mathfrak{h}_s(|\bar{p}_k|). \quad (4.49)$$

For the reader's convenience, we supply the matrix elements $\mathcal{K}_{k,k'}^{\mathfrak{h}}$ for $1 \leq Q \leq 200$ as supplemental material (more details can be found in Appendix C).

C. Numerical method

In order to numerically solve the lattice Boltzmann equation (4.1), we employ an explicit finite difference scheme based on the total variation diminishing (TVD) third-order Runge-Kutta (RK-3) method^{57–61} and the fifth order weighted essentially non-oscillatory (WENO-5) scheme^{54,61–65}.

1. Time stepping

In order to apply the RK-3 method, Eq. (4.1) can be written as:

$$\partial_t f_k = L[f]_k, \quad L[f]_k = -\frac{pk}{m} \partial_x f_k + mg(\partial_p f)_k - \frac{1}{\tau} (f_k - f_k^{(\text{eq})}), \quad (4.50)$$

where the advective term $\frac{pk}{m} \partial_x f_k$ is discussed in Subsec. IV C 2, while the momentum derivative is computed as follows:

$$(\partial_p f)_k = \sum_{k'=1}^{\mathcal{Q}} \mathcal{K}_{k,k'} f_{k'}. \quad (4.51)$$

When the full-range Gauss-Hermite quadrature is employed, $\mathcal{Q} = Q$ and the kernel $\mathcal{K}_{k,k'}$ is given in Eq. (4.23). In the cases when the Gauss-Laguerre and half-range Gauss-Hermite

	$\bar{\omega}_1$	$\bar{\omega}_2$	$\bar{\omega}_3$
$\sigma_1 = \sigma_2 = \sigma_3$	0.1	0.6	0.3
$\sigma_2 = \sigma_3 = 0$	0	2/3	1/3
$\sigma_3 = \sigma_1 = 0$	1/4	0	3/4
$\sigma_1 = \sigma_2 = 0$	1/7	6/7	0
$\sigma_1 = 0$	1	0	0
$\sigma_2 = 0$	0	1	0
$\sigma_3 = 0$	0	0	1

TABLE II. The weighting factors $\bar{\omega}_q$ (4.58) as one, two or all three values of σ_s vanish.

are employed, $\mathcal{Q} = 2Q$ and the corresponding kernels $\mathcal{K}_{k,k'}^L$ and $\mathcal{K}_{k,k'}^h$ are given in Eqs. (4.46) and (4.48), respectively.

We discretise the time coordinate using the time step δt . The total variation diminishing (TVD) preserving RK-3 method proposed in Refs. 54, 57–61, and 66 requires three steps of the form (4.50), which can be summarised as follows:

$$\begin{aligned}
f_k^{(1)} &= f_k(t) + \delta t L[f]_k, \\
f_k^{(2)} &= \frac{3}{4} f_k(t) + \frac{1}{4} f_k^{(1)} + \frac{1}{4} \delta t L[f^{(1)}]_k, \\
f(t + \delta t)_k &= \frac{1}{3} f_k + \frac{2}{3} f_k^{(2)} + \frac{2}{3} \delta t L[f^{(2)}]_k.
\end{aligned} \tag{4.52}$$

The Butcher tableau associated to the above scheme is given in Tab. I.

2. Advection

The domain between the left and right walls is discretised using N_x nodes. In order to better capture the macroscopic profiles in the vicinity of the boundaries, we follow Refs. 66–68 and employ the stretching of the coordinate system induced by the following transformation:

$$x(\eta) = \frac{L}{2A} \tanh \eta, \tag{4.53}$$

where $A \in (0, 1)$ controls the degree of stretching. We construct the spatial grid by employing N_x equidistant values of $\eta \in [-\arctanh A, \arctanh A]$, i.e.:

$$\eta_i = \left(i - \frac{N_x + 1}{2} \right) \delta \eta, \quad \delta \eta = \frac{2}{N_x} \arctanh A, \tag{4.54}$$

where $i = 1, 2, \dots, N_x$. The coarsest part of the resulting grid lies near $x = 0$, while the densest part lies near the two boundaries located at $x = \pm L/2$.

We now write the advection term using the fluxes $\mathcal{F}_{i\pm 1/2}$ as follows:

$$\left(\frac{p_k}{m} \partial_x f_k\right)_i \simeq \frac{\mathcal{F}_{k;i+1/2} - \mathcal{F}_{k;i-1/2}}{x(\eta_{i+1/2}) - x(\eta_{i-1/2})}, \quad (4.55)$$

where $\eta_{i\pm 1/2} = \eta_i \pm \delta\eta/2$, while $x(\eta_{i\pm 1/2})$ is defined through Eq. (4.53) and $\delta\eta$ is given in Eq. (4.54). In this paper, we employ the fifth-order weighted essentially non-oscillatory (WENO-5) scheme^{54,61-66} for the computation of the fluxes $\mathcal{F}_{i\pm 1/2}$. For completeness, we summarise our implementation of the WENO-5 scheme below.

Without loss of generality, we consider the case when $p_k > 0$. The flux $\mathcal{F}_{k;i+1/2}$ can be written as:

$$\mathcal{F}_{k;i+1/2} = \bar{\omega}_1 \mathcal{F}_{k;i+1/2}^1 + \bar{\omega}_2 \mathcal{F}_{k;i+1/2}^2 + \bar{\omega}_3 \mathcal{F}_{k;i+1/2}^3, \quad (4.56)$$

where the interpolating functions $\mathcal{F}_{k;i+1/2}^q$ are given by:

$$\begin{aligned} \mathcal{F}_{k;i+1/2}^1 &= \frac{p_k}{m} \left(\frac{1}{3} f_{k;i-2} - \frac{7}{6} f_{k;i-1} + \frac{11}{6} f_{k;i} \right), \\ \mathcal{F}_{k;i+1/2}^2 &= \frac{p_k}{m} \left(-\frac{1}{6} f_{k;i-1} + \frac{5}{6} f_{k;i} + \frac{1}{3} f_{k;i+1} \right), \\ \mathcal{F}_{k;i+1/2}^3 &= \frac{p_k}{m} \left(\frac{1}{3} f_{k;i} + \frac{5}{6} f_{k;i+1} - \frac{1}{6} f_{k;i+2} \right), \end{aligned} \quad (4.57)$$

while the weighting factors $\bar{\omega}_q$ are defined as:

$$\bar{\omega}_q = \frac{\tilde{\omega}_q}{\tilde{\omega}_1 + \tilde{\omega}_2 + \tilde{\omega}_3}, \quad \tilde{\omega}_q = \frac{\delta_q}{\sigma_q^2}. \quad (4.58)$$

The ideal weights δ_q are:

$$\delta_1 = 1/10, \quad \delta_2 = 6/10, \quad \delta_3 = 3/10, \quad (4.59)$$

while the indicator of smoothness functions σ_q ($q = 1, 2, 3$) are given by:

$$\begin{aligned} \sigma_1 &= \frac{13}{12} (f_{k;i-2} - 2f_{k;i-1} + f_{k;i})^2 + \frac{1}{4} (f_{k;i-2} - 4f_{k;i-1} + 3f_{k;i})^2, \\ \sigma_2 &= \frac{13}{12} (f_{k;i-1} - 2f_{k;i} + f_{k;i+1})^2 + \frac{1}{4} (f_{k;i-1} - f_{k;i+1})^2, \\ \sigma_3 &= \frac{13}{12} (f_{k;i} - 2f_{k;i+1} + f_{k;i+2})^2 + \frac{1}{4} (3f_{k;i} - 4f_{k;i+1} + f_{k;i+2})^2. \end{aligned} \quad (4.60)$$

It is customary to add a small quantity ε (usually taken as 10^{-6}) in the denominators of $\tilde{\omega}_q$ to avoid divisions by 0. However, as pointed out in Ref. 59, the effect of this alteration of

the indicators of smoothness is strongly dependent on the given problem, since ε becomes a dimensional quantity. Furthermore, the accuracy of the resulting scheme depends on the value of ε . Since at higher orders, the distribution functions corresponding to large velocities can have values which are significantly smaller than those for smaller velocities, we cannot predict the effect of employing a unitary value for ε for all distributions. Therefore, we prefer to follow Refs. 61 and 66 and compute the limiting values of $\tilde{\omega}_q$ when one, two or all three of the indicators of smoothness vanish, as indicated in Tab. II.

3. *Boundary conditions*

In this paper, we only consider the case of full diffuse reflection boundary conditions (i.e. corresponding to full accommodation at the walls). We implement these boundary conditions by ensuring that the flux of particles returning into the fluid domain through the cell interface between the fluid and the wall follows a Maxwellian distribution. For definiteness, let us consider the case of the left wall, in which case the above condition reads:

$$\mathcal{F}_{k;1/2} = f_+^{(\text{eq})} \frac{p_k}{m}, \quad (p_k/m > 0), \quad (4.61)$$

where $f_+^{(\text{eq})}$ represents the Maxwell-Boltzmann distribution of the emergent particles [this is defined later in Eq. (5.3)]. The flux in Eq. (4.61) can be achieved analytically by populating the ghost nodes at $i = -2, -1$ and 0 according to:

$$f_{-2;k} = f_{-1;k} = f_{0;k} = f_+^{(\text{eq})}, \quad (p_k/m > 0). \quad (4.62)$$

With the above definitions, Eq. (4.60) shows that $\sigma_1 = 0$ for $i = 0$. According to Tab. II, $\bar{\omega}_1 = 1$ and $\bar{\omega}_2 = \bar{\omega}_3 = 0$ when $\sigma_1 = 0$. Thus, Eq. (4.56) implies that

$$\mathcal{F}_{k;1/2} = \mathcal{F}_{k;1/2}^1 = f_{k;0} \frac{p_k}{m}. \quad (4.63)$$

Thus, Eq. (4.61) is established.

In order to calculate the fluxes at $i = 1/2$ and $i = 3/2$ for particles travelling towards the wall ($p_k < 0$), a quadratic extrapolation is used:

$$\begin{aligned} f_{k;0} &= 3f_{k;1} - 3f_{k;2} + f_{k;3}, \\ f_{k;-1} &= 6f_{k;1} - 8f_{k;2} + 3f_{k;3}, \end{aligned} \quad (4.64)$$

$(p_k < 0).$

Finally, mass conservation is ensured by requiring that:

$$\sum_{k=1}^Q \mathcal{F}_{k;1/2} = 0. \quad (4.65)$$

This translates into the following equation for the particle number density n_+ of the emergent particles:

$$n_+ = -\frac{\sum_{p_k < 0} \mathcal{F}_{k;1/2}}{\sum_{p_k > 0} g_k^+}, \quad (4.66)$$

where $g_k^+ = f_+^{(\text{eq})}/n_+$ is introduced in Eq. (4.19) for the full-range Gauss-Hermite quadrature and in Eq. (4.41) for the case when half-range quadratures are employed.

D. Notation

The models considered in this paper have three free parameters: the type of quadrature (we will only consider the full-range Gauss-Hermite and the half-range Gauss-Hermite quadratures in the remainder of this paper); the quadrature order Q ; and the order N of the expansion of the function g in $f^{(\text{eq})}$. To denote an LB model based on the full-range Gauss-Hermite quadrature of order Q (employing Q discrete momentum vectors) and order N for the expansion of $f^{(\text{eq})}$, we will use the notation HLB(N ; Q). A similar model based on the half-range Gauss-Hermite quadrature will be denoted HHLB(N ; Q), but in this case, the size of the momentum set is $\mathcal{Q} = 2Q$, since a number of Q quadrature points is required on each semiaxis.

The significance of the quadrature order Q was discussed for the case of the full-range Gauss-Hermite quadrature in Subsec. IV A 1, while for the case of half-range quadratures (including the half-range Hermite quadrature), more details can be found in Subsec. IV B 1. The significance of the expansion order N of the equilibrium distribution function was explained in Subsecs. IV A 3 and IV B 3 for the case of the full-range Gauss-Hermite quadrature and the half-range quadratures, respectively.

V. NUMERICAL RESULTS

To illustrate the method introduced in section IV, we consider in this paper the problem of a one-dimensional flow between two diffuse reflective boundaries at rest. The flow is

driven by a force derived from a linear potential $V(x) = mgx$, giving rise to a constant force pointing towards the right wall:

$$F = -\partial_x V(x) = -mg, \quad (5.1)$$

where m is the mass of the particles and g is the constant gravitational acceleration.

This section is divided as follows. In Subsec. V A, we discuss the macroscopic equations governing the flow. The particular case when the walls have equal temperatures admits an equilibrium solution which we discuss in Subsec. V B. In Subsec. V C, we validate our models in the Navier-Stokes (small Kn) limit, where both the full-range and the half-range LB models adequately recover the analytic solution. In Subsec. V D, we derive the analytic solution for the free molecular flow regime and demonstrate that in the ballistic regime, the models based on the full-range Gauss-Hermite quadrature are no longer adequate. However, we find that the models based on the half-range Gauss-Hermite quadrature with the force term implemented as described in Sec. IV B 4 correctly recover the analytic solution. In Subsec. V G we make an analysis of the capabilities of the full-range and half-range models to simulate flows in the transition regime.

A. Macroscopic equations

The Boltzmann equation (2.1) in the presence of the force (5.1) can be written as:

$$\partial_t f + \frac{p}{m} \partial_x f - mg \frac{\partial f}{\partial p} = -\frac{1}{\tau} (f - f^{(\text{eq})}). \quad (5.2)$$

Fixing the origin of the coordinate system at $x = 0$, the channel walls are located at $x_+ = -L/2$ and $x_- = L/2$, where f obeys diffuse reflection boundary conditions:

$$f(x_+, p > 0) = f_+^{(\text{eq})} = n_+ g_+, \quad f(x_-, p < 0) = f_-^{(\text{eq})} = n_- g_-,$$

$$g_{\pm} = \frac{1}{\sqrt{2\pi m T_{\pm}}} \exp\left(-\frac{p^2}{2m T_{\pm}}\right). \quad (5.3)$$

In the above, $f_{\pm}^{(\text{eq})}$ are the Maxwell-Boltzmann distributions (2.2) for the particles emerging from the wall, defined using the particle number densities n_{\pm} , the vanishing velocity of the walls and the wall temperatures T_{\pm} . The densities n_{\pm} at the walls can be computed by

requiring that the mass fluxes through the boundaries vanish, cf. (4.66):

$$n_+ = -\frac{\int_{-\infty}^0 f(x_+, p) p dp}{\int_0^{\infty} g(0, T_+; p) p dp}, \quad n_- = -\frac{\int_0^{\infty} f(x_-, p) p dp}{\int_0^{\infty} g(0, T_-; p) p dp}, \quad (5.4)$$

where $g(u, T; p)$ is defined in Eq. (2.2).

In the stationary state, Eq. (5.2) reduces to:

$$\frac{p}{m} \partial_x f - mg \frac{\partial f}{\partial p} = -\frac{1}{\tau} (f - f^{(\text{eq})}). \quad (5.5)$$

Multiplying the above equation by 1, p and p^2 and integrating with respect to p yields:

$$\partial_x(nu) = 0, \quad (5.6a)$$

$$\partial_x(nT + \rho u^2) = -\rho g, \quad (5.6b)$$

$$\partial_x \left(q_x + \frac{3}{2} nuT + \frac{1}{2} \rho u^3 \right) = -\rho u g, \quad (5.6c)$$

where $\rho = nm$ is the mass density, while the particle number density n , macroscopic velocity u , temperature T and heat flux q are obtained as moments of f , as follows:

$$\begin{aligned} n &= \int_{-\infty}^{\infty} dp f, & u &= \frac{1}{n} \int_{-\infty}^{\infty} dp p f, \\ T &= \frac{1}{nm} \int_{-\infty}^{\infty} dp (p - mu)^2 f, & q &= \int_{-\infty}^{\infty} dp \frac{(p - mu)^3}{2m^2} f. \end{aligned} \quad (5.7)$$

Furthermore, $n(x)$ can be used to compute the total number of particles in the channel, defined as:

$$\mathcal{N} = \int_{-L/2}^{L/2} dx n(x). \quad (5.8)$$

Since $u = 0$ on the boundaries, Eq. (5.6a) implies that $u(x) = 0$ throughout the channel, such that the remaining two equations reduce as follows:

$$\partial_x(nT) = -nmg, \quad (5.9a)$$

$$q = \text{const.} \quad (5.9b)$$

B. Equal wall temperatures

When the two walls are at the same temperature $T_+ = T_- = T_w$, complete thermal equilibrium is achieved in the stationary state for all values of the relaxation time τ . Indeed,

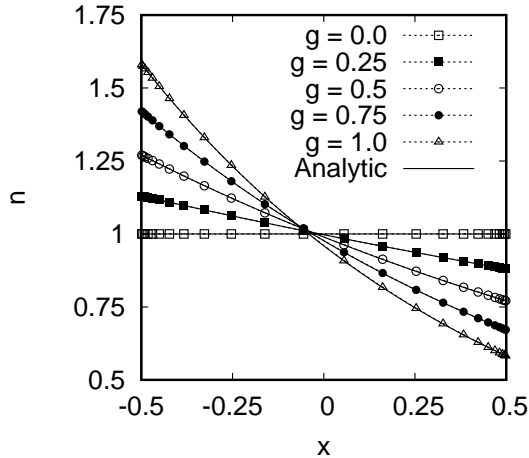


FIG. 3. Density profiles (dashed lines with points) at equilibrium ($T_- = T_+$) for the case when the potential has the linear form in Eq. (5.1), obtained at $\text{Kn} = 0.5$ using the HLB(4;5) model (see Sec. IVD for more details on this notation), compared with the analytic solution (lines) given in Eq. (5.11). Excellent agreement was found for all values of the gravitational constant g considered here.

setting $T = T_w$ in Eq. (5.9a) yields:

$$f = \frac{n(x)}{\sqrt{2\pi m T_w}} \exp\left(-\frac{p^2}{2m T_w}\right), \quad (5.10)$$

where

$$n(x) = \frac{mg\mathcal{N}}{2T_w \sinh \frac{mgL}{2T_w}} \exp\left(-\frac{mgx}{T_w}\right). \quad (5.11)$$

The constant \mathcal{N} represents the total number of particles between the walls and is defined in (5.8). It can be checked that the above solution satisfies the Boltzmann equation (5.2) for any value of τ .

Since the analytic result does not depend on the value of Kn , we have chosen $\text{Kn} = 0.5$ to validate our models. Our numerical results obtained using the HLB(4;5) model (see Sec. IVD for more details on this notation) are compared with the analytic expression (5.11) in Fig. 3 and an excellent agreement can be observed. In our simulations, we used a number of $N_x = 24$ nodes stretched according to Eq. (4.53) with stretching parameter $A = 0.99$. The time step was set to $\delta t = 10^{-3}$.

C. Different wall temperatures: Hydrodynamic regime

At small values of Kn, the flow is close to equilibrium and the Chapman-Enskog expansion can be employed to obtain an approximate solution of the Boltzmann equation^{69–71}. The heat flux can be computed using Fourier’s law:

$$q = -\kappa_T \partial_x T, \quad \kappa_T = \frac{3\tau n T}{2m}. \quad (5.12)$$

In this paper, we consider the following model for the relaxation time¹⁶:

$$\tau = \frac{\text{Kn}}{n}, \quad (5.13)$$

such that Eq. (5.9b) can be rearranged as follows:

$$\partial_x T^2 = A, \quad (5.14)$$

where A is a constant. The solution of the above equation is:

$$T(x) = \sqrt{Ax + B}, \quad (5.15)$$

where the constants A and B are determined by the boundary conditions:

$$A = \frac{T_-^2 - T_+^2}{L}, \quad B = \frac{T_-^2 + T_+^2}{2}. \quad (5.16)$$

It is remarkable that, in the Navier-Stokes limit, the temperature profile does not depend on g . More generally, it can be shown that $T(x)$ does not depend on the form of the potential $V(x)$. Substituting Eq. (5.15) into Eq. (5.12) yields:

$$q(x) = \frac{3\text{Kn}}{4mL}(T_+^2 - T_-^2). \quad (5.17)$$

To find the expression for the particle number density n , Eq. (5.9a) can be integrated, yielding:

$$n(x) = \frac{mg\mathcal{N}}{2T(x) \sinh \frac{mgL}{T_+ + T_-}} \exp \left[-\frac{mgL}{T_-^2 - T_+^2} [2T(x) - T_- - T_+] \right], \quad (5.18)$$

where the total number of particles \mathcal{N} is defined in Eq. (5.8). It can be checked that Eq. (5.18) reduces to Eq. (5.11) when $T_- = T_+ = T_w$.

Figures 4(a) and (b) show a comparison between our numerical results and the analytic expression (5.18) obtained for n in the Navier-Stokes regime (\mathcal{N} was set to 1), for various

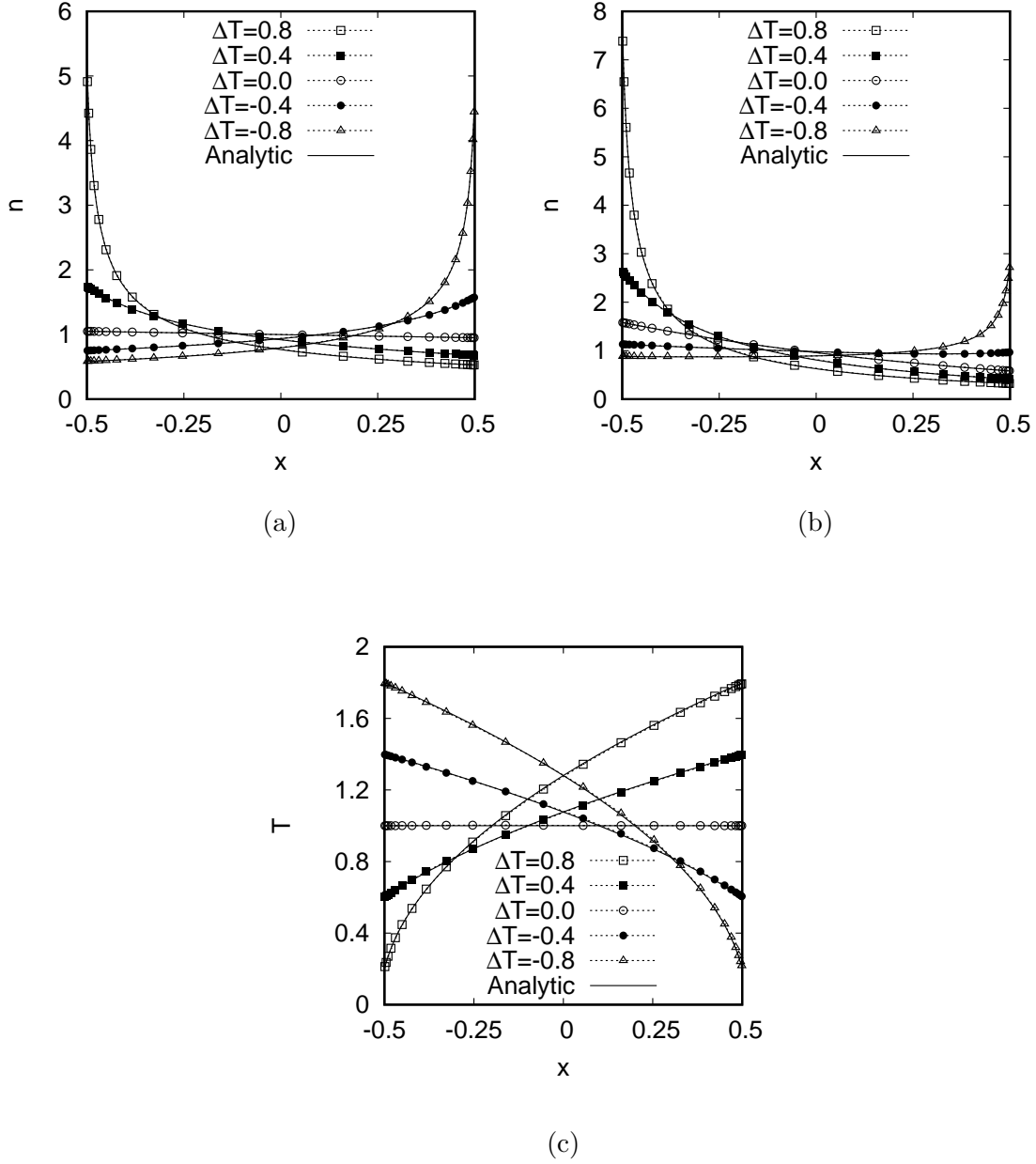


FIG. 4. Navier-Stokes regime ($\text{Kn} = 10^{-3}$): Comparison between the density n (top) and temperature T (bottom) profiles obtained using the HLB(4;5) model (dashed lines with points) and the analytic solutions (5.11) and (5.15), respectively (contiguous lines). The plots for n correspond to the accelerations $g = 0.1$ (left) and $g = 1.0$ (right). Since the temperature profile in the Navier-Stokes regime does not depend on the potential (i.e. on the value of g), (c) displays only the case when $g = 1.0$. The curves correspond to various temperature differences $\Delta T = (T_- - T_+)/2$ between the left and right walls.

values of the temperature difference $\Delta T = (T_- - T_+)/2$ and for two values of the gravitational acceleration: $g = 0.1$ and $g = 1.0$. In both cases, the agreement is excellent. Since in the Navier-Stokes limit, the temperature does not depend on g , Fig. 4(c) compares the temperature profile obtained using our models and the analytic expression in Eq. (5.15) only for the case when $g = 1.0$. Also in this case, it can be seen that the agreement is excellent. The numerical results were obtained using the HLB(4; 5) model (this notation is explained in Sec. IV D). The time step was set to $\delta t = 10^{-4}$, the fluid domain was discretised using $N_x = 24$ nodes and we performed 5.000.000 iterations to ensure that the stationary state was achieved.

D. Ballistic regime: analytic analysis

Let us consider the stationary solutions of the Boltzmann equation in the ballistic regime, when the right hand side of Eq. (5.5) vanishes:

$$\frac{p}{m} \partial_x f - mg \partial_p f = 0, \quad (5.19)$$

where f obeys the diffuse reflection boundary conditions (5.3). During free-streaming, the total energy (Hamiltonian) of each particle, defined through:

$$H = V(x) + \frac{p^2}{2m}, \quad (5.20)$$

is conserved. Indeed, it can be checked that H satisfies Eq. (5.19), since $\partial_x H = mg$ and $\partial_p H = p/m$.

The distribution function can be written as:

$$f(x, p) = \theta_+ f^+ + \theta_- f^-, \quad (5.21a)$$

where (θ_+, θ_-) are Heaviside step functions which reduce to $(1, 0)$ and $(0, 1)$ on the left and right walls, respectively. The functions $f^\pm \equiv f^\pm(x, p)$ are completely determined by the diffuse reflection boundary conditions (5.3), together with the requirement that the Hamiltonian (5.20) an invariant of the Boltzmann equation:

$$f^+ = \frac{n_+}{\sqrt{2\pi m T_+}} \exp \left\{ -\frac{1}{T_+} \left[\frac{p^2}{2m} + V(x) - V(x_+) \right] \right\}, \quad (5.21b)$$

$$f^- = \frac{n_-}{\sqrt{2\pi m T_-}} \exp \left\{ -\frac{1}{T_-} \left[\frac{p^2}{2m} + V(x) - V(x_-) \right] \right\}, \quad (5.21c)$$

where n_{\pm} and T_{\pm} represent the densities and temperatures of the walls.

In order to find the form of the arguments of θ_{\pm} , we note that the potential $V(x) = mgx$ has a maximum on the right wall. For a given position x , three situations can occur: a) the particle has a negative momentum, such that the particle will travel to the left boundary; (b) the particle is travelling rightwards and its kinetic energy is larger than the potential difference between the right wall and its current location: in this case, the particle will hit the right wall; (c) the momentum of the particle is positive, however the value of its Hamiltonian H is smaller than the potential at the right boundary: this implies that the particle will reach a minimum approach with respect to the right wall, after which its momentum will become negative and its behaviour will be similar to the one described for case (a). This suggests that θ_+ and θ_- can be written as:

$$\theta_+ \equiv \theta(p + m\sqrt{g(L-2x)}), \quad \theta_- \equiv \theta(-p - m\sqrt{g(L-2x)}). \quad (5.22)$$

Indeed, substituting $\theta_{\pm} \equiv \theta(p \pm \sqrt{2m[a_{\pm} - V(x)]})$ instead of f in Eq. (5.19) gives:

$$\begin{aligned} & \left(\frac{p}{m} \frac{\partial}{\partial x} - mg \frac{\partial}{\partial p} \right) \theta(\pm p \pm m\sqrt{g(L-2x)}) \\ & = \mp \sqrt{\frac{g}{L-2x}} \delta[\pm p \pm m\sqrt{g(L-2x)}] [p + m\sqrt{g(L-2x)}]. \end{aligned} \quad (5.23)$$

It can be seen that the right hand side of the above equation vanishes due to the presence of the delta function.

Thus, the full solution of the stationary Boltzmann equation in the ballistic regime subject to a force derived from the potential $V(x) = mgx$ is:

$$\begin{aligned} f(x, p) = & \theta[p + m\sqrt{g(L-2x)}] \frac{n_+ e^{-mg(L+2x)/2T_+}}{\sqrt{2\pi m T_+}} e^{-p^2/2mT_+} \\ & + \theta[-p - m\sqrt{g(L-2x)}] \frac{n_- e^{mg(L-2x)/2T_-}}{\sqrt{2\pi m T_-}} e^{-p^2/2mT_-}. \end{aligned} \quad (5.24)$$

The mass flux inside the channel is given by:

$$\int_{-\infty}^{\infty} dp f p = \sqrt{\frac{m}{2\pi}} \left(n_+ \sqrt{T_+} e^{-2mgL/T_+} - n_- \sqrt{T_-} \right), \quad (5.25)$$

which is constant, as expected from the continuity equation. In order to prevent mass transfer through the boundaries, the constants n_{\pm} must satisfy:

$$n_- \sqrt{T_-} = n_+ e^{-mgL/T_+} \sqrt{T_+}. \quad (5.26)$$

The particle number density can be found by substituting Eq. (5.24) into Eq. (5.7):

$$n(x) = \frac{n_+}{2} e^{-mg(L+2x)/2T_+} \operatorname{erfc} \left(-\sqrt{\frac{mg(L-2x)}{2T_+}} \right) + \frac{n_-}{2} e^{mg(L-2x)/2T_-} \operatorname{erfc} \left(\sqrt{\frac{mg(L-2x)}{2T_-}} \right). \quad (5.27)$$

The constant n_+ can be found by considering the total number of particles \mathcal{N} inside the channel, which is defined in Eq. (5.8). Using the following formula:

$$\int_0^a dz e^z \operatorname{erf} \sqrt{z} = e^a \operatorname{erf} \sqrt{a} - 2\sqrt{\frac{a}{\pi}}, \quad (5.28)$$

the total number of particles \mathcal{N} can be expressed in terms of n_{\pm} :

$$\mathcal{N} = \frac{n_+ T_+}{2mg} e^{-mgL/T_+} \left[e^{mgL/T_+} \operatorname{erfc} \left(-\sqrt{\frac{mgL}{T_+}} \right) - 1 \right] + \frac{n_- T_-}{2mg} \left[e^{mgL/T_-} \operatorname{erfc} \left(\sqrt{\frac{mgL}{T_-}} \right) - 1 \right]. \quad (5.29)$$

Using Eq. (5.26), the following expressions for n_- and n_+ can be obtained:

$$n_- \sqrt{T_-} = n_+ \sqrt{T_+} e^{-mgL/T_+} = \frac{2mg\mathcal{N}}{\sqrt{T_+} \left[e^{mgL/T_+} \operatorname{erfc} \left(-\sqrt{\frac{mgL}{T_+}} \right) - 1 \right] + \sqrt{T_-} \left[e^{mgL/T_-} \operatorname{erfc} \left(\sqrt{\frac{mgL}{T_-}} \right) - 1 \right]}. \quad (5.30)$$

Thus, the particle number density can be written as:

$$n(x) = mg\mathcal{N} \frac{\frac{1}{\sqrt{T_+}} e^{\frac{mg(L-2x)}{2T_+}} \operatorname{erfc} \left(-\sqrt{\frac{mg(L-2x)}{2T_+}} \right) + \frac{1}{\sqrt{T_-}} e^{\frac{mg(L-2x)}{2T_-}} \operatorname{erfc} \left(\sqrt{\frac{mg(L-2x)}{2T_-}} \right)}{\sqrt{T_+} \left[e^{mgL/T_+} \operatorname{erfc} \left(-\sqrt{\frac{mgL}{T_+}} \right) - 1 \right] + \sqrt{T_-} \left[e^{mgL/T_-} \operatorname{erfc} \left(\sqrt{\frac{mgL}{T_-}} \right) - 1 \right]}. \quad (5.31)$$

An expression for the temperature can be obtained using Eq. (5.7):

$$\frac{nT}{2} = n_+ e^{-mgL/T_+} e^{mg(L-2x)/2T_+} \int_{-m\sqrt{g(L-2x)}}^{\infty} \frac{dp}{\sqrt{2\pi mT_+}} \frac{p^2}{2m} e^{-p^2/2mT_+} + n_- e^{mg(L-2x)/2T_-} \int_{-\infty}^{-m\sqrt{g(L-2x)}} \frac{dp}{\sqrt{2\pi mT_-}} \frac{p^2}{2m} e^{-p^2/2mT_-}. \quad (5.32)$$

Using the following property:

$$\frac{2}{\sqrt{\pi}} \int_a^{\infty} dz z^2 e^{-z^2} = \frac{a}{\sqrt{\pi}} e^{-a^2} + \frac{1}{2} \operatorname{erfc}(a), \quad (5.33)$$

the final expression for $T(x)$ can be obtained:

$$T(x) = \frac{\sqrt{T_+} e^{\frac{mg(L-2x)}{2T_+}} \operatorname{erfc}\left(-\sqrt{\frac{mg(L-2x)}{2T_+}}\right) + \sqrt{T_-} e^{\frac{mg(L-2x)}{2T_-}} \operatorname{erfc}\sqrt{\frac{mg(L-2x)}{2T_-}}}{\frac{1}{\sqrt{T_+}} e^{\frac{mg(L-2x)}{2T_+}} \operatorname{erfc}\left(-\sqrt{\frac{mg(L-2x)}{2T_+}}\right) + \frac{1}{\sqrt{T_-}} e^{\frac{mg(L-2x)}{2T_-}} \operatorname{erfc}\sqrt{\frac{mg(L-2x)}{2T_-}}}. \quad (5.34)$$

The heat flux can be obtained using Eq. (5.7):

$$\begin{aligned} q(x) &= \frac{n_- \sqrt{T_-}}{\sqrt{2\pi m}} (T_+ - T_-) \\ &= \frac{g \mathcal{N}(T_+ - T_-) \sqrt{2m/\pi}}{\sqrt{T_+} \left[e^{\frac{mgL}{T_+}} \operatorname{erfc}\left(-\sqrt{\frac{mgL}{T_+}}\right) - 1 \right] + \sqrt{T_-} \left[e^{\frac{mgL}{T_-}} \operatorname{erfc}\left(\sqrt{\frac{mgL}{T_-}}\right) - 1 \right]} \end{aligned} \quad (5.35)$$

It can be checked that n (5.31), T (5.34) and q (5.35) satisfy Eqs. (5.6). In the limit $T_- = T_+ = T_w$, n reduces to Eq. (5.11), while $T(x) \rightarrow T_w$ and $q \rightarrow 0$.

E. Ballistic regime: HLB vs HHLB

We now set $g = 0.1$ and $\Delta T = (T_- - T_+)/2 = -0.4$. Because the left wall has a higher temperature than the right wall (i.e. $T_+ = 1.4$ compared to $T_- = 0.6$), the gas particles tend to accumulate on the right wall. On the other hand, the gravitational force ($g = 0.1$) acts from right to left, inducing an accumulation of particles on the left wall. The result is a non-trivial particle distribution having a minimum in the central region of the channel and local maxima in the vicinity of the walls. Our numerical results for the particle number density n and temperature T are compared in Fig. 5 with the corresponding analytic expressions (5.31) and (5.34), respectively. Throughout this section, all simulation results presented were obtained using a time step of $\delta t = 10^{-4}$ on a grid of $N_x = 24$ points. The stretching parameter in Eq. (4.53) is $A = 0.99$.

The plots on the left of Fig. 5 show the numerical results obtained using the full-range Gauss-Hermite models HLB(N ; Q) for $Q \in \{20, 50, 100, 500\}$ and $N = \min(20, Q - 1)$. At low quadrature orders, the density profile obtained using the HLB models decreases monotonically from the left to the right wall, in qualitative contrast to the analytic prediction. At $Q = 500$, the density profile obtained using the HLB model is closer to the analytic prediction, but it presents non-physical oscillations, such that its shape is still qualitatively incorrect. The temperature profile decreases monotonically from the left wall to the right wall for all quadrature orders, as required analytically. The temperature on the walls slowly

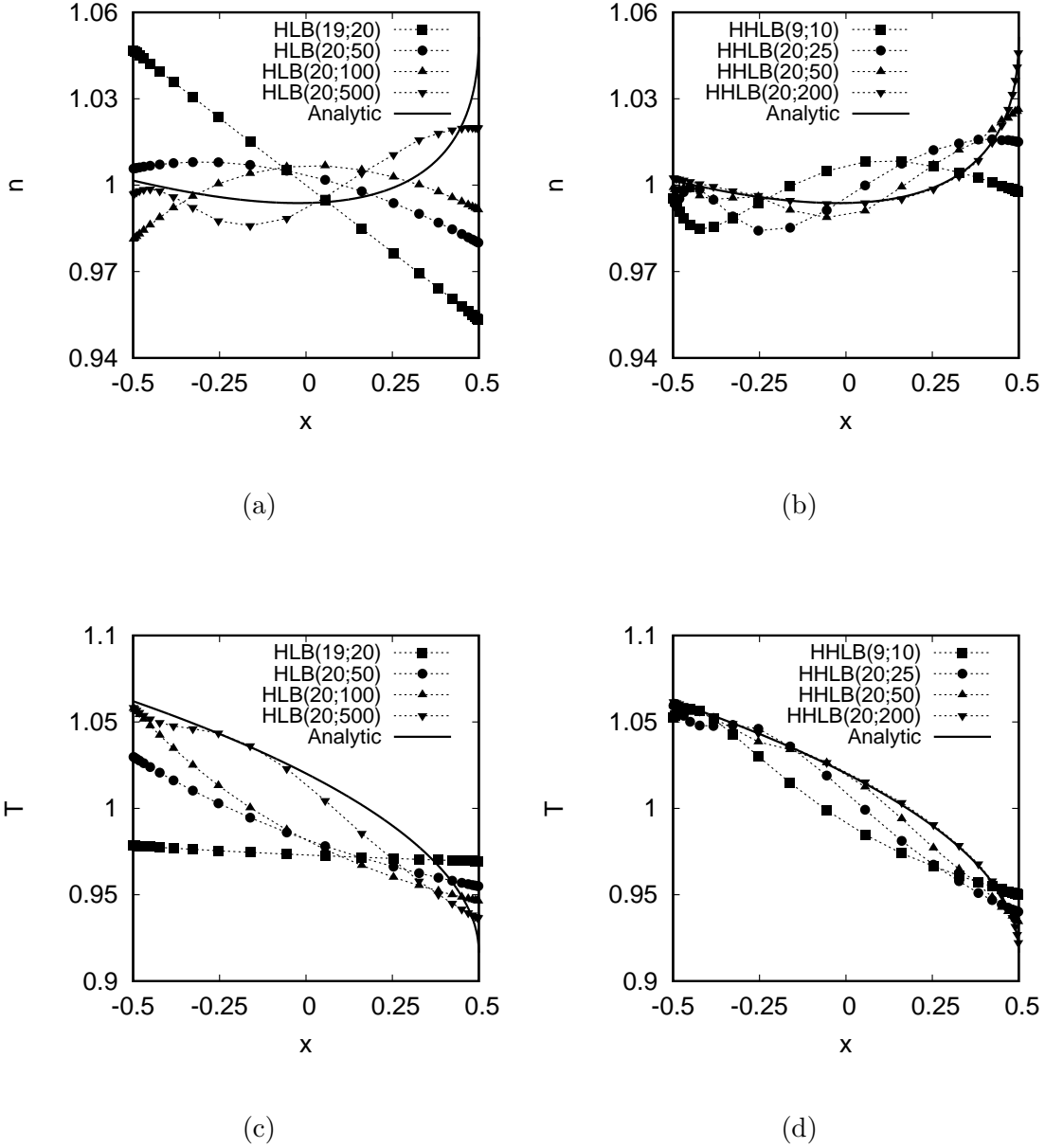


FIG. 5. Density (top) and temperature (bottom) profiles in the ballistic regime for $g = 1.0$ and $\Delta T = (T_- - T_+)/2 = -0.4$, obtained using the HLB (left) and HHLB (right) models. The numerical results are shown using dashed lines and points, while the analytic solutions (5.31) and (5.34), are shown using continuous lines.

approaches the analytic value from below (above) on the left (right) wall, indicating that the temperature jump is overestimated at low quadrature orders. The temperature profile

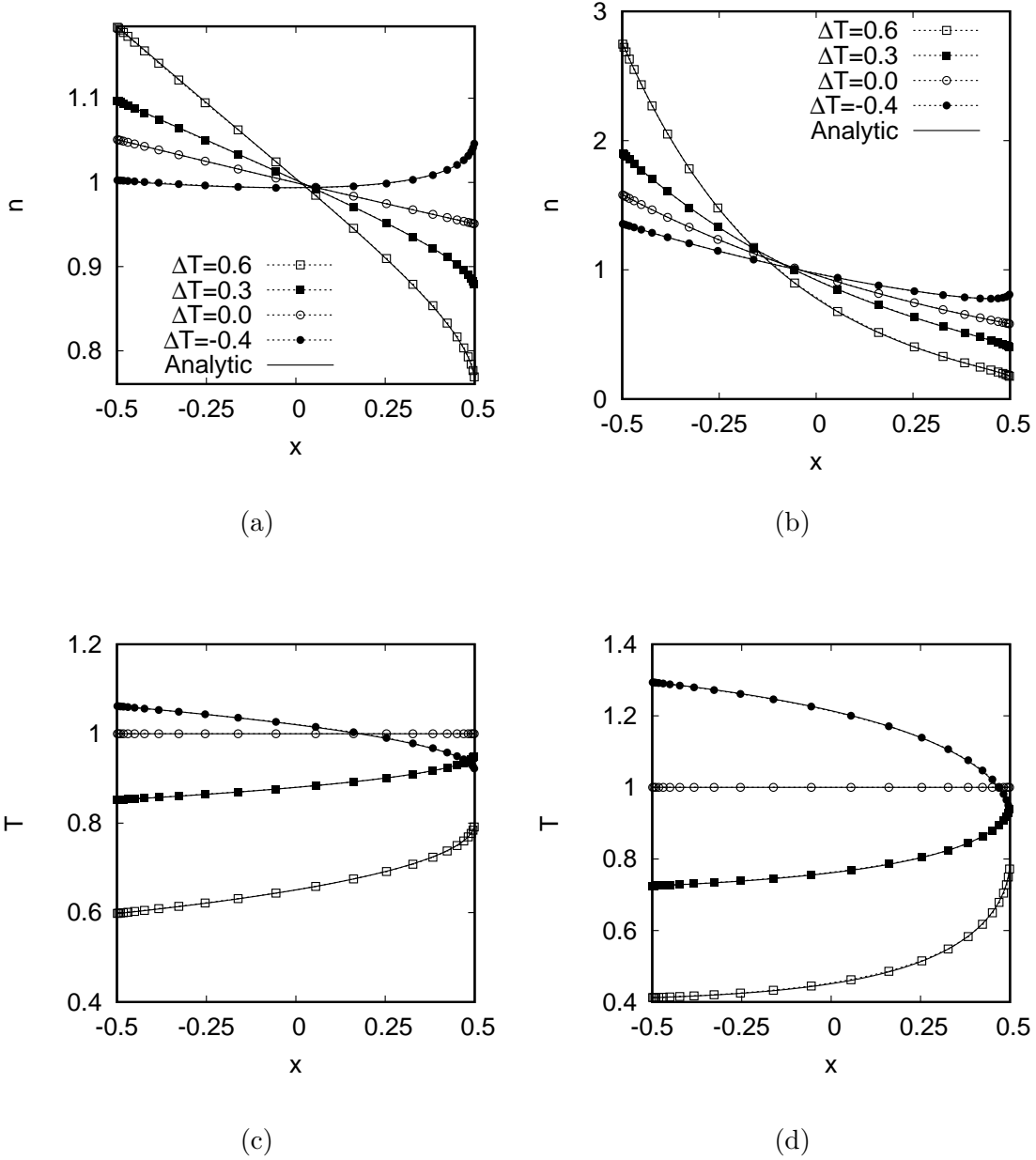


FIG. 6. Density (top) and temperature (bottom) profiles in the ballistic regime for $g = 0.1$ (left) and $g = 1.0$ (right). The curves correspond to various values of $\Delta T = (T_- - T_+)/2$. The numerical results are shown using dashed lines and points, being in excellent agreement with the analytic solutions (5.31) and (5.34), which are shown using continuous lines.

in the bulk still does not approach the form of the analytic profile even when $Q = 500$.

The numerical results obtained in the same condition as described above using the half-

range Gauss-Hermite models HHLB($N; Q$) (employing a number of $Q = 2Q$ velocities) with $Q \in \{10, 25, 50, 200\}$ and $N = \min(20, Q - 1)$ are presented in the plots on the right in Fig. 5. While even at low quadrature orders, the results obtained using the HHLB models are closer to the analytic prediction than those obtained using the HLB models, the resulting profiles exhibit unphysical oscillations. The quadrature order at which these oscillations disappear seems to depend on the grid size, as will be demonstrated later. It is important to note that when $Q = 200$, the agreement between the numerical and the analytic results is excellent.

The plots in Fig. 6 show a comparison between our simulation results obtained using the HHLB(20;200) model and the analytic profiles in Eqs. (5.31) and (5.34) for $g = 0.1$ (left) and $g = 1$ (right) at $\Delta T = (T_- - T_+)/2 \in \{0.6, 0.3, 0.0, -0.4\}$. It can be seen that the agreement between our numerical solutions and the analytic profiles is excellent for all tested values of g and ΔT . A more quantitative analysis of the accuracy of our method is discussed in the following subsection.

F. Ballistic regime: convergence tests

To gain some quantitative insight on the convergence properties of our LB models, we follow Refs. 40 and 41 and perform the convergence test described below. First, we fix as reference profiles $M_{\text{ref}} \in \{n_{\text{ref}}, T_{\text{ref}}\}$ the profiles corresponding to the analytic solutions (5.31) and (5.34), evaluated at the points corresponding to our chosen grid. The convergence of our models is tested by analysing the relative error between the profiles obtained using our models and the reference profiles. We introduce for a given profile $M \in \{n, T\}$ the error $\varepsilon(M)$ through:

$$\varepsilon(M) = \frac{\max_x [M(x) - M_{\text{ref}}(x)]}{\max\{\max_x [M(x)] - \min_x [M(x)], 0.1\}}. \quad (5.36)$$

where the denominator measures the spread of $M(x)$ (i.e. the difference between the maximum and the minimum values of $M(x)$), bounded from below by 0.1. In this paper, we consider that convergence is achieved when the error $\varepsilon(M)$ is less than 1% for all $M \in \{n, T\}$, i.e.:

$$\varepsilon_{\text{max}} \equiv \max_{M \in \{n, T\}} \varepsilon(M) < 0.01. \quad (5.37)$$

Figure 7(a) shows that the error ε_{max} decreases with the number of grid points N_x for $N_x \lesssim 36$. The increase in ε_{max} as N_x is further increased is due to the development of spurious oscillations which seem to increase in amplitude as N_x is increased at fixed values

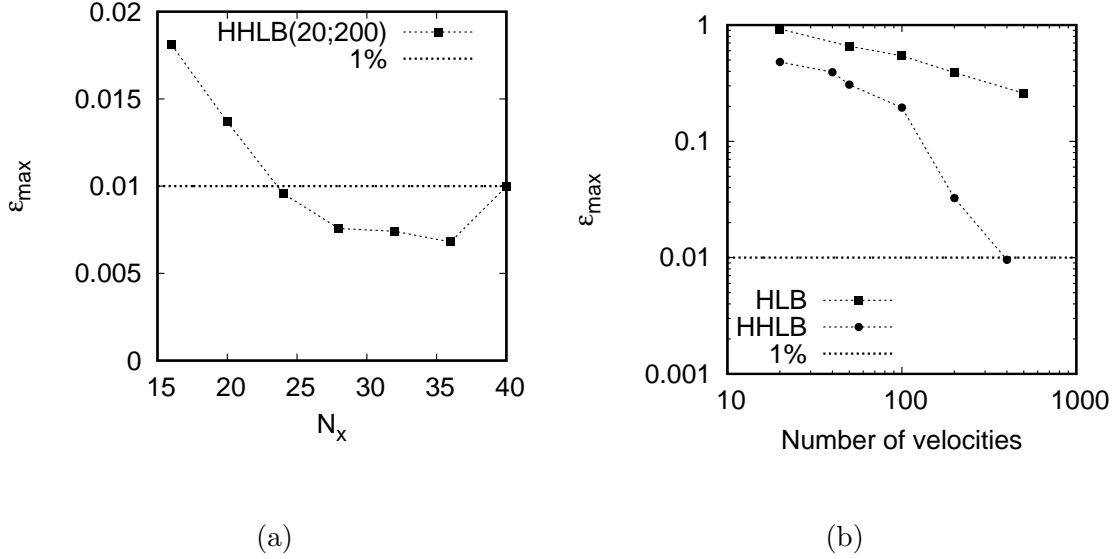


FIG. 7. Relative error ε_{\max} (5.37) with respect to the analytic profiles in the free-streaming regime of: (a) the results obtained with the HHLB(20;200) model as a function of the number of grid points N_x ; (b) the results obtained using the models HLB(N ; Q) and HHLB(N ; Q) at $N_x = 24$ as a function of the number of velocities (Q for the HLB models and $2Q$ for the HHLB models).

of Q . In Fig. 7(b), we fix $N_x = 24$ and study the dependence of ε_{\max} on the quadrature order Q for the HLB(N ; Q) and the HHLB(N ; Q) models, where $N = \min(20, Q - 1)$. It can be seen that the error in the HLB models decreases at a much slower rate than the error corresponding to the HHLB models.

G. Transition regime

In Subsec. VC we validated our implementation of the force term by comparing our numerical results for the particle number density n and temperature T in the Navier-Stokes regime with the analytic results (5.18) and (5.15), respectively. Next, we have shown in Subsec. VF that the HHLB(N ; Q) models based on the half-range Gauss-Hermite quadrature can reproduce, at large enough values of the quadrature Q , the analytic solutions (5.31) and (5.34) for n and T in the ballistic regime. At the same time, we have shown that in the ballistic regime, the HLB(N ; Q) based on the full-range Gauss-Hermite models exhibit a

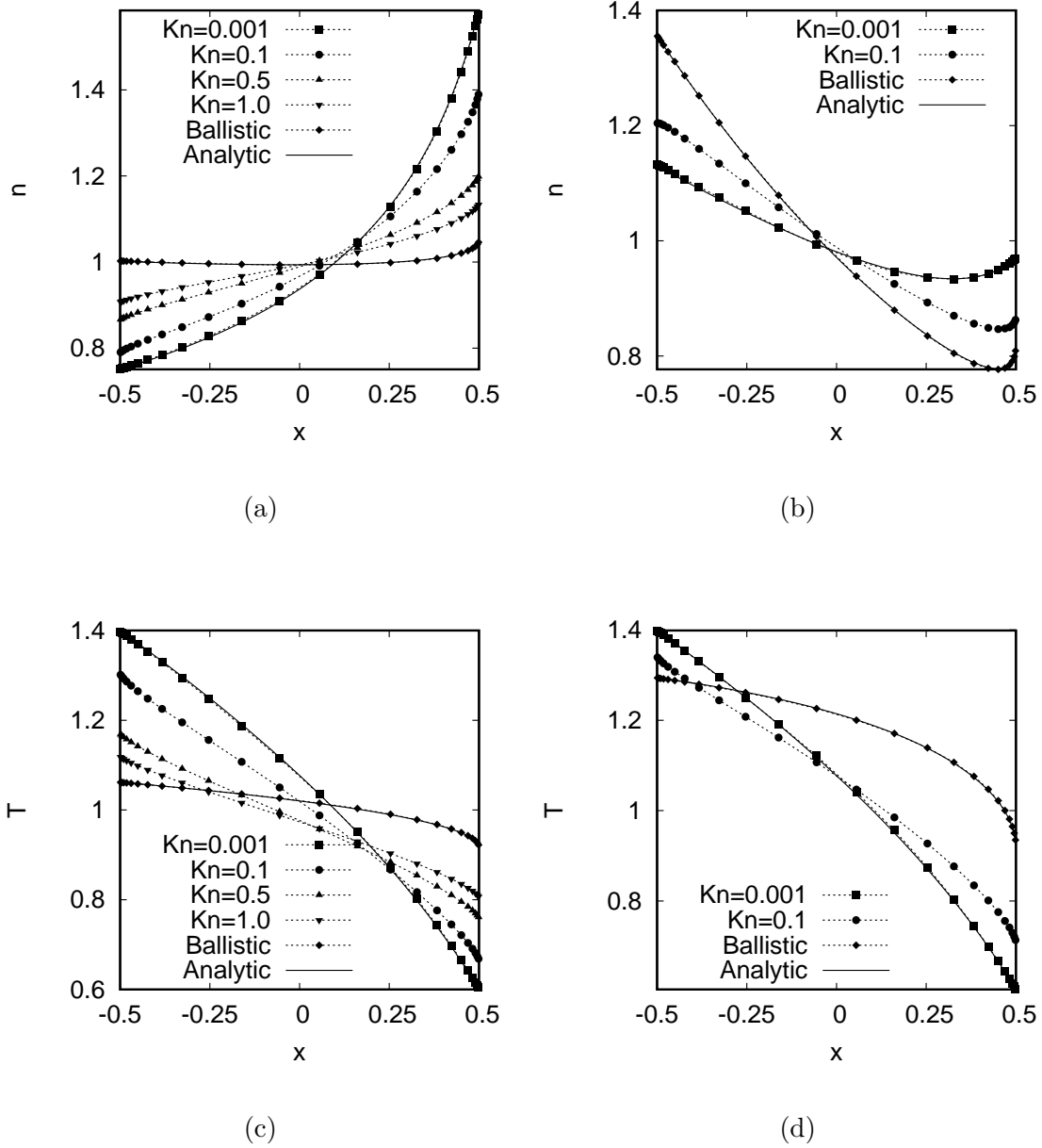


FIG. 8. Density (top) and temperature (bottom) profiles obtained using our LB models (dotted lines and points) when $g = 0.1$ (left) and $g = 1.0$ (right). The analytic formulae represented using contiguous lines are given by Eqs. (5.18) (n) and (5.15) (T) in the hydrodynamic regime and by Eqs. (5.31) (n) and (5.34) (T) in the ballistic regime.

slow convergence towards the analytic solutions, with the error obtained using the test introduced in Refs. 40 and 41 and described in Eq. (5.37) being $\varepsilon_{\max} \simeq 25.9\%$ with respect

to the analytic solution even at $Q = 500$.

In this section, we attempt to analyse the ability of the HLB and HHLB models to simulate flows in the transition regime. In the absence of an analytic solution of the Boltzmann-BGK equation (2.1) or of results obtained using other methods, we will limit the analysis to employing the convergence test introduced in Subsec. V F, but in this case with respect to the reference profiles obtained using the HHLB(20;200) model. According to Fig. 7, this model produces profiles which are within the 1% error limit of the analytic solution in the ballistic regime.

Figure 8 shows the numerical results obtained using our models at various values of the Knudsen number Kn . At $\text{Kn} = 0.001$, the numerical results obtained using the HLB(4;5) model are compared with the analytic solutions derived in Subsec. V C. In the ballistic regime, the numerical results obtained using the HHLB(20;200) model are compared with the analytic solutions derived in Subsec. V D. In the transition regime $\text{Kn} \in \{0.1, 0.5, 1\}$, the numerical results represented in Fig. 8 were obtained using the HHLB(20;200) model.

Taking as reference the profiles obtained using the HHLB(20;200) model at $N_x = 24$ nodes and a time step $\delta t = 10^{-4}$, we test the convergence of the HLB(N ; Q) and HHLB(N ; Q) models in the transition regime as Q is increased, with $N = \min(Q - 1, 20)$. Figure 9 shows the error ε_{\max} (5.37) computed with respect to the reference profiles. It can be seen that the results obtained using the HLB(N ; Q) models unambiguously converge towards the reference profiles, but the error at a fixed number of velocities is always larger than when the HHLB(N ; Q) models are considered. Out of the six convergence tests that we conducted, the HLB(N ; Q) models managed to satisfy the 1% convergence test only in three cases, namely $(g, \text{Kn}) \in \{(0.1, 0.1), (0.1, 0.5), (1, 0.1)\}$, failing when $(g, \text{Kn}) \in \{(0.1, 1), (1, 0.5), (1, 1)\}$ for all tested $Q \leq 500$. It can be seen that at fixed Kn , the convergence of the HLB and HHLB models is slower as g is increased.

VI. CONCLUSION

In this paper, we have presented a systematic procedure for the construction of lattice Boltzmann models based on half-range quadratures for force-driven flows in confined geometries. In order to ensure the correct recovery of the zeroth order half-range moment of the momentum derivative $\partial_p f$ of the distribution function, we have shown that the theory

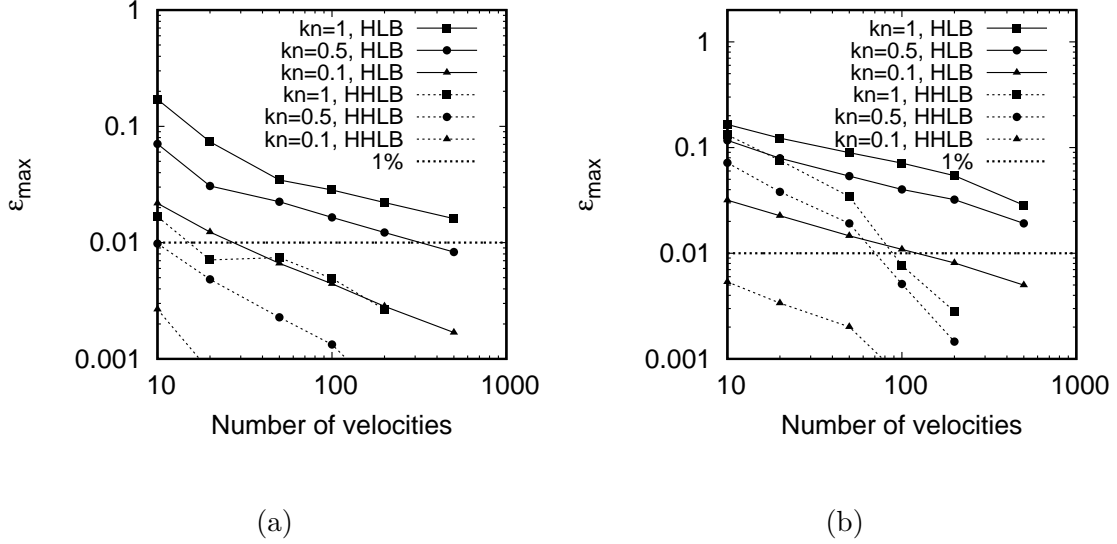


FIG. 9. Total error ε_{\max} (5.37) computed with respect to the reference profiles obtained using the HHLB(20; 200) model for $\text{Kn} = 0.5$ (dotted lines with points) and $\text{Kn} = 1.0$ (continuous lines with points) when $g = 0.1$ (left) and $g = 1.0$ (right). The error ε_{\max} is shown as a function of the number of velocities $\mathcal{Q} = Q$ and $2Q$ for the HLB(N ; Q) and HHLB(N ; Q) models, respectively.

of distributions must be employed in order to cope with the potential discontinuity of the distribution function f at $p = 0$.

In order to validate our proposed scheme, we have considered the problem of a gas under the action of gravity (i.e. $V(x) = mgx$, where g is the constant gravitational acceleration) between two diffuse-reflecting walls. We validated our models using analytic solutions in three regimes: in the isothermal regime (i.e. the walls have equal temperature); in the Navier-Stokes regime; and in the ballistic regime. In order for our models to accurately reproduce the analytic solutions, we employ a grid stretching algorithm which allows the mesh to be refined near the boundaries, where the gradients of the macroscopic fields are in general steeper. In all cases, our simulation results reproduce to high accuracy the analytic predictions.

While in the isothermal and Navier-Stokes regimes, the models based on the full-range Gauss-Hermite quadrature are sufficiently accurate to reproduce the analytic solution, as the value of Kn is increased, half-range capabilities are required in order to deal with the

discontinuity of the distribution function induced by the boundaries. In the ballistic regime, we were able to reduce the error with respect to the analytic solution to less than 1% on a grid consisting of $N_x = 24$ nodes by using the HHLB(20;200) model, which employs an expansion of order $N = 20$ of the equilibrium distribution function $f^{(\text{eq})}$ and a quadrature order $Q = 200$. Our convergence test showed that the error of the HLB(N ; Q) models based on the full-range Gauss-Hermite quadrature compared to the analytic result was over 25% even when $Q = 500$.

We further performed an analysis of the properties of our models in the transition regime, at $\text{Kn} = 0.5$ and $\text{Kn} = 1$. Since no analytic solution was available in this regime, we performed a convergence study by taking the results obtained using the HHLB(20;200) model as reference profiles. Our analysis showed that the error ε_{max} in the profiles obtained using the HLB(N ; Q) models with respect to the reference profiles decreases monotonically as Q is increased. The value of ε_{max} stays larger than 1% for $\text{Kn} \in \{0.5, 1\}$ when $g = 1$ for all $Q \leq 500$, while when $g = 0.1$, we were able to reduce ε_{max} under 1% at $Q = 500$ only for $\text{Kn} = 0.5$.

In this paper, we have only considered the academic example of a constant force acting between two walls which have different temperatures. However, the purpose of this paper is to introduce the formalism necessary to implement the momentum derivative of the distribution function when half-range quadratures are employed. Furthermore, the example considered in this paper was taken for simplicity to be one-dimensional. While we highlight in Appendix A that the methodology is easily extendible to higher dimensions, we defer further validation tests for future publications. A direct application of the formalism introduced in this paper can be found in Ref. 66, where the circular Couette flow between concentric cylinders is considered.

ACKNOWLEDGMENTS

This work was supported by a grant of the Romanian National Authority for Scientific Research, CNCS-UEFISCDI, project number PN-II-ID-JRP-2011-2-0060 and by the ANR DEPART project, Grant ANR-12-IS04-0003-01 of the French Agence Nationale de la Recherche.

Appendix A: Extension to multiple dimensions

In d dimensions, the Boltzmann equation (2.1) becomes:

$$\partial_t f + \frac{\mathbf{p}}{m} \cdot \nabla f + \mathbf{F} \cdot (\nabla_{\mathbf{p}} f) = -\frac{1}{\tau}(f - f^{(\text{eq})}). \quad (\text{A1})$$

The numerical solution of Eq. (A1) can be obtained following the same steps described in Sec. IV, which we summarise in what follows. We refer to the resulting models as mixed quadrature lattice Boltzmann models, following Refs. 40 and 41. For definiteness, we will always refer to the case $d = 3$. Since there is no direct generalisation of one-dimensional advection schemes, we will restrict the discussion in this appendix to the discretisation of the momentum space (Sec. A 1), the construction of $f^{(\text{eq})}$ (Sec. A 2) and the construction of the force term (Sec. A 2 a).

1. Discretisation of the momentum space

In the mixed quadrature lattice Boltzmann models, the momentum space is constructed using a direct product rule. This allows the quadrature on each axis to be constructed independently by taking into account the characteristics of the flow, as employed, e.g., in for the 2D Couette⁴⁰, 2D Poiseuille⁴¹ and 3D Couette⁴² flows.

Since in this paper we propose a Cartesian split of the momentum space, the elements of the discrete set of momentum vectors can be written as $\mathbf{p}_{ijk} = (p_{x,i}, p_{y,j}, p_{z,k})$. The indices i , j and k run from 1 to \mathcal{Q}_α ($\alpha \in \{x, y, z\}$), where $\mathcal{Q}_\alpha = Q_\alpha$ or $\mathcal{Q}_\alpha = 2Q_\alpha$ when a full-range or half-range quadrature of order Q_α is employed on the α axis. The distribution function f_{ijk} corresponding to the momentum vector \mathbf{p}_{ijk} is linked to the Boltzmann distribution function through the direct extension of Eq. (4.6):

$$f_{ijk} = \left(\frac{w_i^x p_{0,x}}{\omega(p_{x,i})} \right) \left(\frac{w_j^y p_{0,y}}{\omega(p_{y,j})} \right) \left(\frac{w_k^z p_{0,z}}{\omega(p_{z,k})} \right) f^{Q_x, Q_y, Q_z}(p_{x,i}, p_{y,j}, p_{z,k}). \quad (\text{A2})$$

The weights w_s^α are given by Eq. (4.5) for the case of the full-range Gauss-Hermite quadrature and by Eq. (4.31) when the half-range Gauss-Laguerre or Gauss-Hermite quadratures are employed, respectively.

After the discretisation of the momentum space, Eq. (A1) becomes:

$$\partial_t f_{ijk} + \frac{\mathbf{p}_{ijk}}{m} \cdot \nabla f_{ijk} + \mathbf{F} \cdot (\nabla_{\mathbf{p}} f)_{ijk} = -\frac{1}{\tau}(f_{ijk} - f_{ijk}^{(\text{eq})}). \quad (\text{A3})$$

2. Expansion of the equilibrium distribution function

The Maxwell-Boltzmann equilibrium distribution can be factorised with respect to the Cartesian axes as follows^{40–42}:

$$f^{(\text{eq})} = n g_x g_y g_z, \quad (\text{A4})$$

where $g_\alpha \equiv g(u_\alpha, T; p_\alpha)$ is defined in Eq. (2.2). After choosing the type of quadrature, the quadrature order Q_α and the expansion order N_α on each axis α , $f_{ijk}^{(\text{eq})}$ is obtained by multiplying the corresponding truncations of $g_{x,i}$, $g_{y,j}$ and $g_{z,k}$:

$$f_{ijk}^{(\text{eq})} = n g_{x,i} g_{y,j} g_{z,k}, \quad (\text{A5})$$

where $g_{\alpha,s}$ is given by Eqs. (4.19) and (4.41) when the full-range Gauss-Hermite quadrature and half-range quadratures are employed.

a. Force term

In order to implement the force term in multiple dimensions, the inner product between the force \mathbf{F} and the momentum derivative $\nabla_{\mathbf{p}} f$ can be expanded as follows:

$$\mathbf{F} \cdot \nabla_{\mathbf{p}} f = F_x \partial_{p_x} f + F_y \partial_{p_y} f + F_z \partial_{p_z} f. \quad (\text{A6})$$

Each momentum derivative can be computed using the corresponding kernel function, following the prescription in Eqs. (2.11) and (3.23):

$$\begin{aligned} \partial_{p_x} f &= \int_{-\infty}^{\infty} dp_x \mathcal{K}(p_x, p'_x) f(p'_x, p_y, p_z), \\ \partial_{p_y} f &= \int_{-\infty}^{\infty} dp_y \mathcal{K}(p_y, p'_y) f(p_x, p'_y, p_z), \\ \partial_{p_z} f &= \int_{-\infty}^{\infty} dp_z \mathcal{K}(p_z, p'_z) f(p_x, p_y, p'_z). \end{aligned} \quad (\text{A7})$$

The kernel function $\mathcal{K}(p, p')$ is given in Eqs. (2.12) when the full-range Gauss-Hermite is employed. For a generic half-range quadrature, the kernel function is given in Eq. (3.24).

After the discretisation of the momentum space, the momentum derivatives of f can be

written as:

$$\begin{aligned}
\left(\frac{\partial f}{\partial p_x}\right)_{ijk} &= \sum_{i'=1}^{Q_x} \mathcal{K}_{i,i'} f_{i'jk}, \\
\left(\frac{\partial f}{\partial p_y}\right)_{ijk} &= \sum_{j'=1}^{Q_y} \mathcal{K}_{j,j'} f_{ij'k}, \\
\left(\frac{\partial f}{\partial p_z}\right)_{ijk} &= \sum_{k'=1}^{Q_z} \mathcal{K}_{k,k'} f_{ijk'},
\end{aligned} \tag{A8}$$

where the kernel function $\mathcal{K}_{s,s'}$ for the full-range Gauss-Hermite quadrature is given in Eq. (4.23). For a general half-range quadrature, the kernel is given in Eq. (4.44), while for the specific cases of the Gauss-Laguerre and half-range Gauss-Hermite quadratures, the kernel is given in Eqs. (4.46) and (4.48).

Finally, the analogue of Eq. (A6) after the discretisation of the momentum space reads:

$$\mathbf{F} \cdot (\nabla_{\mathbf{p}} f)_{ijk} = F_x \left(\frac{\partial f}{\partial p_x}\right)_{ijk} + F_y \left(\frac{\partial f}{\partial p_y}\right)_{ijk} + F_z \left(\frac{\partial f}{\partial p_z}\right)_{ijk}. \tag{A9}$$

Appendix B: Half-range orthogonal polynomials

Let $\{\phi_\ell(z)\}$ be the set of polynomials employed in Sec. III, which satisfy the orthogonality relation (3.5) on the domain $[0, \infty)$, forming a complete set in the sense of Eq. (3.7). The polynomial $\phi_\ell(z)$ is of order ℓ in z and admits the following expansion:

$$\phi_\ell(z) = \sum_{s=0}^{\ell} \phi_{\ell,s} z^s, \tag{B1}$$

where $\phi_{\ell,s}$ are constant coefficients. In particular, it can be seen that:

$$\phi_\ell(0) = \phi_{\ell,0}. \tag{B2}$$

The derivative of $\phi_\ell(z)$ with respect to z is a polynomial of order $\ell - 1$, which can be expressed with respect to the (complete) set $\{\phi_\ell(z)\}$ as follows:

$$\phi'_\ell(z) = - \sum_{s=0}^{\ell-1} \varphi_{\ell,s} \phi_s(z), \tag{B3}$$

where $\varphi_{\ell,s}$ are constant coefficients. The minus sign was inserted for future convenience.

In the construction of the momentum derivative of the distribution function f , it will be useful to compute the expansion of the derivative of $\omega(z)\phi_\ell(z)$ in the following form:

$$\frac{\partial[\omega(z)\phi_\ell(z)]}{\partial z} = \omega(z) \sum_{s=0}^{\infty} \frac{1}{\gamma_s} \psi_{\ell,s} \phi_s(z), \quad (\text{B4})$$

where $\psi_{\ell,s}$ can be calculated as in Eq. (3.6), using an integration by parts:

$$\psi_{\ell,s} = -\omega(0)\phi_\ell(0)\phi_s(0) + \sum_{j=0}^{s-1} \varphi_{s,j} \langle \phi_\ell, \phi_j \rangle. \quad (\text{B5})$$

Equation (B3) was used to eliminate $\phi'_s(x)$. The inner product above vanishes for all values of j which are smaller than ℓ . Hence, it only contributes to $\psi_{\ell,s}$ when $s > \ell$. Substituting the above result back into Eq. (B4), the following result can be obtained:

$$\frac{\partial[\omega(z)\phi_\ell(z)]}{\partial z} = -\omega(z)\omega(0)\phi_{\ell,0} \sum_{s=0}^{\infty} \frac{1}{\gamma_s} \phi_{s,0}\phi_s(z) + \omega(z)\gamma_\ell \sum_{s=\ell+1}^{\infty} \frac{1}{\gamma_s} \varphi_{s,\ell}\phi_s(z). \quad (\text{B6})$$

Let us now specialise the above to the case of the half-range Hermite polynomials $\{\mathfrak{h}_\ell(z)\}$, for which the weight function $\omega(z)$ and norm γ_ℓ have the following expressions:

$$\omega(z) = \frac{1}{\sqrt{2\pi}} e^{-z^2/2}, \quad \gamma_\ell = 1. \quad (\text{B7})$$

The coefficients $\varphi_{\ell,s}$ introduced in Eq. (B3) can be obtained by multiplying Eq. (B3) by $\omega(z)\phi_s(z)$ and integrating with respect to z :

$$\varphi_{\ell,s} = \omega(0)\mathfrak{h}_{\ell,0}\mathfrak{h}_{s,0} - \langle \mathfrak{h}_\ell, z\mathfrak{h}_s \rangle + \langle \mathfrak{h}_\ell, \mathfrak{h}'_s \rangle, \quad (\text{B8})$$

where an integration by parts was used. Since \mathfrak{h}'_s is a polynomial of order $s-1 < \ell$, the last term in the above equality vanishes. To evaluate the second term, the following recursion relation can be employed⁴⁰:

$$\mathfrak{h}_{s+1}(z) = (a_s z + b_s)\mathfrak{h}_s(z) + c_s \mathfrak{h}_{s-1}(z). \quad (\text{B9})$$

Since $s < \ell$, \mathfrak{h}_ℓ is orthogonal on \mathfrak{h}_s and \mathfrak{h}_{s-1} , allowing Eq. (B8) to be written as:

$$\varphi_{\ell,s} = \omega(0)\mathfrak{h}_{\ell,0}\mathfrak{h}_{s,0} - \frac{1}{a_s} \delta_{\ell,s+1}, \quad (\text{B10})$$

where a_s is given by⁴⁰:

$$a_s = \frac{\mathfrak{h}_{s+1,s+1}}{\mathfrak{h}_{s,s}}. \quad (\text{B11})$$

Appendix C: Note on supplemental material

The supplemental material available at the publisher’s website consists of a collection of data files organised as follows.

The files `roots-herm.txt`, `weights-herm.txt`, `roots-hh.txt` and `weights-hh.txt` contain the roots of the full-range and half-range Hermite polynomials employed in this paper, as well as their corresponding weights. Each of these files comprise 200 lines corresponding to $1 \leq Q \leq 200$. Line Q consists of Q entries corresponding to the roots or weights for the quadrature order Q , as follows:

$$\begin{array}{c} x_{1,1} \\ x_{2,1} \ x_{2,2} \\ x_{3,1} \ x_{3,2} \ x_{3,3} \\ \dots \end{array}$$

In the above, $x_{Q,k}$ represents the k 'th root or weight for quadrature order Q .

The files `kharm-Q*.dat` contain, for a given value of Q , the $Q \times Q$ matrix elements of the kernel $\mathcal{K}_{k,k'}^H$ (4.23). The files consist of Q rows corresponding to $1 \leq k \leq Q$ with Q entries each, corresponding to $1 \leq k' \leq Q$:

$$\begin{array}{cccc} \mathcal{K}_{1,1}^H & \mathcal{K}_{1,2}^H & \dots & \mathcal{K}_{1,Q}^H \\ \mathcal{K}_{2,1}^H & \mathcal{K}_{2,2}^H & \dots & \mathcal{K}_{2,Q}^H \\ \dots & \dots & \dots & \dots \\ \mathcal{K}_{Q,1}^H & \mathcal{K}_{Q,2}^H & \dots & \mathcal{K}_{Q,Q}^H \end{array}$$

Finally, the files `khh-Q*.dat` contain, for a given value of Q , the $2Q \times 2Q$ matrix elements of the kernel $\mathcal{K}_{k,k'}^h$ (4.44), with $1 \leq k \leq 2Q$ and $1 \leq k' \leq 2Q$. The (k') 'th element on line k corresponds to $\mathcal{K}_{k,k'}^h$.

REFERENCES

- ¹M. G. el Haq, MEMS Applications, CRC Press, Boca Raton, 2006.
- ²P. Tabeling, Introduction to Microfluidics (English translation), Oxford University Press, Oxford, 2011.
- ³H. A. Stone, S. Kim, Microfluidics: Basic issues, applications, and challenges, AIChE Journal 47 (2001) 1250–1254. doi:10.1002/aic.690470602.

- ⁴A. V. Delgado, *Interfacial Electrokinetics and Electrophoresis*, CRC Press, New York, 2001.
- ⁵Voldman, Electrical forces for microscale cell manipulation, *Annual Review of Biomedical Engineering* 8 (2006) 425–454. doi:10.1146/annurev.bioeng.8.061505.095739.
- ⁶P. Fede, V. Sofonea, R. Fournier, S. Blanco, O. Simonin, G. Lepoutère, V. E. Ambruş, Lattice Boltzmann model for predicting the deposition of inertial particles transported by a turbulent flow, *Int. J. Multiph. Flow* 76 (2015) 187–197. doi:10.1016/j.ijmultiphaseflow.2015.07.004.
- ⁷R. Balescu, *Aspects of anomalous transport in plasmas*, IOP Publishing Ltd, Cornwall (UK), 2005.
- ⁸B. Piaud, S. Blanco, R. Fournier, V. E. Ambruş, V. Sofonea, Gauss quadratures - the keystone of lattice Boltzmann models, *Int. J. Mod. Phys. C* 25 (2014) 1340016. doi:10.1142/S0129183113400160.
- ⁹X. W. Shan, X. F. Yuan, H. D. Chen, Kinetic theory representation of hydrodynamics: a way beyond the Navier-Stokes equation, *J. Fluid. Mech.* 550 (2006) 413–441. doi:10.1017/S0022112005008153.
- ¹⁰M. O. Deville, T. B. Gatski, *Mathematical Modeling for Complex Fluids and Flows*, Springer, Berlin, 2012.
- ¹¹H. Grad, *Principles of the Kinetic Theory of Gases*, Vol. XII of *Encyclopedia of Physics* (editor: S. Flügge), Springer, Berlin, 1958.
- ¹²Y. Sone, *Kinetic Theory and Fluid Dynamics*, Birkhäuser, Boston, 2002.
- ¹³G. Karniadakis, A. Beskok, N. Aluru, *Microflows and Nanoflows: Fundamentals and Simulation*, Springer, Berlin, 2005.
- ¹⁴H. Struchtrup, *Macroscopic Transport Equations for Rarefied Gas Flows*, Springer, Berlin, 2005.
- ¹⁵C. Shen, *Rarefied Gas Dynamics: Fundamentals, Simulations and Micro Flows*, Springer, Berlin, 2005.
- ¹⁶Y. Sone, *Molecular Gas Dynamics: Theory, Techniques and Applications*, Birkhäuser, Boston, 2007.
- ¹⁷J. C. Maxwell, On stresses in rarified gases arising from inequalities of temperature, *Philos. Trans. R. Soc. London* 170 (1879) 231–256.
- ¹⁸J. P. Meng, Y. H. Zhang, Accuracy analysis of high-order lattice Boltzmann models for rar-

- efied gas flows, *J. Comput. Phys.* 230 (2011) 835–849. doi:10.1016/j.jcp.2010.10.023.
- ¹⁹S. Ansumali, I. V. Karlin, Kinetic boundary conditions in the lattice Boltzmann method, *Phys. Rev. E* 66 (2002) 026311. doi:10.1103/PhysRevE.66.026311.
- ²⁰J. P. Meng, Y. H. Zhang, Gauss-Hermite quadratures and accuracy of lattice Boltzmann models for nonequilibrium gas flows, *Phys. Rev. E* 83 (2011) 036704. doi:10.1103/PhysRevE.83.036704.
- ²¹J. P. Meng, Y. H. Zhang, X. W. Shan, Multiscale lattice Boltzmann approach to modeling gas flows, *Phys. Rev. E* 83 (2011) 046701. doi:10.1103/PhysRevE.83.046701.
- ²²J. P. Meng, Y. H. Zhang, N. G. Hadjiconstantinou, G. A. Radtke, X. W. Shan, Lattice ellipsoidal statistical BGK model for thermal non-equilibrium flows, *J. Fluid. Mech.* 718 (2013) 347–370. doi:10.1017/jfm.2012.616.
- ²³V. E. Ambruş, V. Sofonea, High-order thermal lattice Boltzmann models derived by means of Gauss quadrature in the spherical coordinate system, *Phys. Rev. E* 86 (2012) 016708. doi:10.1103/PhysRevE.86.016708.
- ²⁴J. Y. Yang, J. C. Huang, L. Tsuei, Numerical solutions of the nonlinear model Boltzmann equations, *Proc. R. Soc. Lond. A* 448 (1995) 55–80. doi:10.1098/rspa.1995.0003.
- ²⁵Z.-H. Li, H.-X. Zhang, Numerical investigation from rarefied flow to continuum by solving the boltzmann model equation, *Int. J. Numer. Meth. Fluids* 42 (2003) 361–382. doi:10.1002/flid.517.
- ²⁶Z.-H. Li, H.-X. Zhang, Study on gas kinetic unified algorithm for flows from rarefied transition to continuum, *J. Comput. Phys* 193 (2004) 708–738. doi:10.1016/j.jcp.2003.08.022.
- ²⁷S. Lorenzani, L. Gibelli, A. Frezzotti, A. Frangi, C. Cercignani, Kinetic approach to gas flows in microchannels, *Nanoscale and Microscale Thermophysical Engineering* 11 (2007) 211–226. doi:10.1080/15567260701333489.
- ²⁸Z.-H. Li, H.-X. Zhang, Gas-kinetic numerical studies of three-dimensional complex flows on spacecraft re-entry, *J. Comput. Phys* 228 (2009) 1116–1138. doi:10.1016/j.jcp.2008.10.013.
- ²⁹A. Frezzotti, L. Gibelli, B. Franzelli, A moment method for low speed microflows, *Continuum Mech. Thermodyn.* 21 (2009) 495–509. doi:10.1007/s00161-009-0128-y.
- ³⁰A. Frezzotti, G. P. Ghiroldi, L. Gibelli, Solving the Boltzmann equation on GPUs, *Comput. Phys. Comm.* 182 (2011) 2445–2453. doi:10.1016/j.cpc.2011.07.002.

- ³¹L. Gibelli, Velocity slip coefficients based on the hard-sphere Boltzmann equation, *Phys. Fluids* 24 (2012) 022001. doi:10.1063/1.3680873.
- ³²Z. Guo, K. Xu, R. Wang, Discrete unified gas kinetic scheme for all Knudsen number flows: Low-speed isothermal case, *Phys. Rev. E* 88 (2013) 033305. doi:10.1103/PhysRevE.88.033305.
- ³³G. P. Ghiroldi, L. Gibelli, A direct method for the Boltzmann equation based on a pseudo-spectral velocity space discretization, *J. Comput. Phys.* 258 (2014) 568–584. doi:10.1016/j.jcp.2013.10.055.
- ³⁴Z. Guo, R. Wang, K. Xu, Discrete unified gas kinetic scheme for all knudsen number flows. ii. thermal compressible case, *Phys. Rev. E* 91 (2015) 033313. doi:10.1103/PhysRevE.91.033313.
- ³⁵G. P. Ghiroldi, L. Gibelli, A finite-difference lattice Boltzmann approach for gas microflows, *Commun. Comput. Phys.* 17 (2015) 1007–1018. doi:10.4208/cicp.2014.m424.
- ³⁶Y. Shi, Y. W. Yap, J. E. Sader, Linearized lattice Boltzmann method for micro- and nanoscale flow and heat transfer, *Phys. Rev. E* 92 (2015) 013307. doi:10.1103/PhysRevE.92.013307.
- ³⁷V. E. Ambruş, V. Sofonea, Application of lattice Boltzmann models based on Laguerre quadratures in complex flows, *Interfac. Phenom. Heat Transfer* 2 (2014) 235–251. doi:10.1615/InterfacPhenomHeatTransfer.2015011655.
- ³⁸V. E. Ambruş, V. Sofonea, Implementation of diffuse-reflection boundary conditions using lattice Boltzmann models based on half-space Gauss-Laguerre quadratures, *Phys. Rev. E* 89 (2014) 041301(R). doi:10.1103/PhysRevE.89.041301.
- ³⁹V. E. Ambruş, V. Sofonea, Lattice Boltzmann models based on Gauss quadratures, *Int. J. Mod. Phys. C* 25 (2014) 1441011. doi:10.1142/S0129183114410113.
- ⁴⁰V. E. Ambruş, V. Sofonea, Lattice Boltzmann models based on half-range Gauss-Hermite quadratures, *J. Comput. Phys.* 316 (2016) 760–788. doi:10.1016/j.jcp.2016.04.010.
- ⁴¹V. E. Ambruş, V. Sofonea, Application of mixed quadrature lattice Boltzmann models for the simulation of Poiseuille flow at non-negligible values of the Knudsen number, *J. Comput. Sci.* doi:10.1016/j.jocs.2016.03.016.
- ⁴²V. E. Ambruş, V. Sofonea, Half-range lattice Boltzmann models for the simulation of Couette flow using the Shakhov collision term, arXiv:1702.01335 [physics.flu-dyn].
- ⁴³N. S. Martys, X. Shan, H. Chen, Evaluation of the external force term in the discrete Boltz-

- mann equation, *Phys. Rev. E* 58 (1998) 6855–6857. doi:10.1103/PhysRevE.58.6855.
- ⁴⁴F. W. J. Olver, D. W. Lozier, R. F. Boisvert, C. W. Clark, *NIST Handbook of Mathematical Functions*, Cambridge University Press, New York, 2010.
- ⁴⁵E. P. Gross, E. A. Jackson, S. Ziering, Boundary value problems in kinetic theory of gases, *Ann. Phys.* 1 (1957) 141–167. doi:10.1016/0003-4916(57)90056-8.
- ⁴⁶I. A. Graur, A. P. Polikarpov, Comparison of different kinetic models for the heat transfer problem, *Heat Mass Transf.* 46 (2009) 237–244. doi:10.1007/s00231-009-0558-x.
- ⁴⁷S. H. Kim, H. Pitsch, I. D. Boyd, Accuracy of higher-order lattice Boltzmann methods for microscale flows with finite Knudsen numbers, *J. Comput. Phys.* 227 (2008) 8655–8671. doi:10.1016/j.jcp.2008.06.012.
- ⁴⁸M. Watari, Finite difference lattice Boltzmann method with arbitrary specific heat ratio applicable to supersonic flow simulations, *Physica A* 382 (2007) 502–522. doi:10.1016/j.physa.2007.03.037.
- ⁴⁹M. Watari, Velocity slip and temperature jump simulations by the three-dimensional thermal finite-difference lattice Boltzmann method, *Phys. Rev. E* 79 (2009) 066706. doi:10.1103/PhysRevE.79.066706.
- ⁵⁰M. Watari, Relationship between accuracy and number of velocity particles of the finite-difference lattice Boltzmann method in velocity slip simulations, *J. Fluid Eng.* 132 (2010) 101401. doi:10.1115/1.4002359.
- ⁵¹Y. Shi, P. L. Brookes, Y. W. Wap, J. E. Sader, Accuracy of the lattice Boltzmann method for low-speed noncontinuum flows, *Phys. Rev. E* 83 (2011) 045701(R). doi:10.1103/PhysRevE.83.045701.
- ⁵²L. de Izarra, J. L. Rouet, B. Izrar, High-order lattice Boltzmann models for gas flow for a wide range of Knudsen numbers, *Phys. Rev. E* 84 (2011) 066705. doi:10.1103/PhysRevE.84.066705.
- ⁵³E. F. Toro, *Riemann Solvers and Numerical Methods for Fluid Dynamics: A Practical Introduction*, 3rd Edition, Springer, Berlin, 2009.
- ⁵⁴L. Rezzolla, O. Zanotti, *Relativistic hydrodynamics*, Oxford University Press, Oxford, UK, 2013.
- ⁵⁵F. B. Hildebrand, *Introduction to Numerical Analysis*, second edition Edition, Dover Publications, 1987.
- ⁵⁶B. Shizgal, *Spectral Methods in Chemistry and Physics: Applications to Kinetic Theory*

- and Quantum Mechanics (Scientific Computation), Springer, 2015.
- ⁵⁷C.-W. Shu, S. Osher, Efficient implementation of essentially non-oscillatory shock-capturing schemes, *J. Comput. Phys.* 77 (1988) 439–471. doi:10.1016/0021-9991(88)90177-5.
- ⁵⁸S. Gottlieb, C.-W. Shu, Total variation diminishing Runge-Kutta schemes, *Math. Comp.* 67 (1998) 73–85. doi:10.1090/S0025-5718-98-00913-2.
- ⁵⁹A. K. Henrick, T. D. Aslam, J. M. Powers, Mapped weighted essentially non-oscillatory schemes: Achieving optimal order near critical points, *J. Comput. Phys.* 207 (2005) 542–567. doi:10.1016/j.jcp.2005.01.023.
- ⁶⁰J. A. Trangenstein, Numerical solution of hyperbolic partial differential equations, Cambridge University Press, New York, USA, 2007.
- ⁶¹R. Blaga, V. E. Ambruş, High-order quadrature-based lattice Boltzmann models for the flow of ultrarelativistic rarefied gases, arXiv:1612.01287 [physics.flu-dyn].
- ⁶²G. S. Jiang, C. W. Shu, Efficient implementation of Weighted ENO schemes, *J. Comput. Phys.* 126 (1996) 202. doi:10.1006/jcph.1996.0130.
- ⁶³C.-W. Shu, High order ENO and WENO schemes for computational fluid dynamics, in: T. J. Barth, H. Deconinck (Eds.), High-order methods for computational physics, Springer-Verlag, Berlin, 1999, pp. 439–582.
- ⁶⁴Y. Gan, A. Xu, G. Zhang, Y. Li, Lattice Boltzmann study on kelvin-helmholtz instability: Roles of velocity and density gradients, *Phys. Rev. E* 83 (2011) 056704. doi:10.1103/PhysRevE.83.056704.
- ⁶⁵K. Hejranfar, M. H. Saadat, S. Taheri, High-order weighted essentially nonoscillatory finite-difference formulation of the lattice Boltzmann method in generalized curvilinear coordinates, *Phys. Rev. E* 95 (2017) 023314. doi:10.1103/PhysRevE.95.023314.
- ⁶⁶S. Busuioc, V. E. Ambruş, Lattice Boltzmann models based on the vielbein formalism for the simulation of the circular Couette flow, arXiv:1708.05944 [physics.flu-dyn].
- ⁶⁷R. Mei, W. Shyy, On the finite difference-based lattice Boltzmann method in curvilinear coordinates, *J. Comput. Phys.* 143 (1998) 426–448. doi:10.1006/jcph.1998.5984.
- ⁶⁸Z. Guo, T. S. Zhao, Explicit finite-difference lattice Boltzmann method for curvilinear coordinates, *Phys. Rev. E* 67 (2003) 066709. doi:10.1103/PhysRevE.67.066709.
- ⁶⁹K. Huang, Statistical Mechanics, Wiley, New York, 1963.
- ⁷⁰S. Harris, An Introduction to the Theory of the Boltzmann Equation, Holt, Rinehart and

Winston, New York, 1971.

⁷¹C. Cercignani, The Boltzmann Equation and Its Applications, Springer-Verlag, New York, 1988.